Proposal to Install a Forward π^0 Detector in STAR

H. M. Spinka, D. G. Underwood,
Argonne National Laboratory
Argonne, IL U. S. A.

J. Balewski, L. C. Bland, W. W. Jacobs, A. Klyachko, M. Planinić, G. Rakness,
T. Rinckel, K. Solberg, J. Sowinski, E. J. Stephenson, S. E. Vigdor, S. W. Wissink,
Indiana University Cyclotron Facility
Bloomington, IN U. S. A.

A. Derevshchikov, Y. Matulenko, A. Meschanin, L. Nogach, S. Nurushev, A. Vasiliev,
Institute of High Energy Physics
Protvino, Russia

Y. Averichev, V. Dunin, L. Efimov, N. Gagunashvili, S. Kulikov, Y. Panebratsev,
E. Potrebenikova, S. Razin, O. Rogachevski, V. Tikhomirov, M. Tokarev, V. Yurevich, A. Zubarev,
Laboratory of High Energy Physics, JINR
Dubna, Russia

B. Anderson, D. Keane, S. Margetis, J. Watson, W. Zhang
Kent State University
Kent, OH U. S. A.

A. Ogawa,
Penn State University, University Park, PA U. S. A.

G. Eppley, B. Llope,
Rice University
Houston, TX U. S. A.

J. Hoffmann, L. Ray,
University of Texas, Austin, TX U. S. A.

C. A. Gagliardi, R. E. Tribble, M. A. Vasiliev,
Texas A & M University
College Station, TX U. S. A.

G. J. Igo, J. Kiryluk and C. A. Whitten Jr.,
UCLA
Los Angeles, CA U. S. A.

February 14, 2001

Abstract

We propose to install a Forward π^0 Detector (FPD) approximately 7.5 m east of the STAR interaction region, consisting of the prototype Endcap Electromagnetic Calorimeter and three sets of Pb-glass detectors. The goal is to measure the single-spin transverse asymmetry (A_N) for leading π^0 production from colliding protons at $\sqrt{s} = 200\,\mathrm{GeV}$, $x_F > 0.4$, and $p_T \approx 1 - 4\,\mathrm{GeV}$, a process which is expected to give rise to a non-zero A_N value on the order of $+0.10$. The FPD is an essential addition to STAR for the first polarized beam collisions. If the theoretical predictions are correct, it can confirm that the colliding beams are polarized, test our ability to make relative luminosity measurements and provide an experimental means of verifying the orientation of the polarization vector at the STAR collision point.

1 Motivation

One of the ultimate goals of the RHIC spin programs at both the PHENIX and STAR detectors is to study the spin structure of the proton. The previous generation of polarized deep inelastic scattering experiments at SLAC and DESY [1], using polarized electron beams, and at CERN [2], using polarized muon beams, have established that the quarks (and antiquarks) account for only a small fraction of the proton's spin. The remainder must arise from either the polarization of the gluons that bind the quarks within the proton, or from the orbital motion of the quarks and gluons. At present, there are only very coarse constraints on the fraction of the proton's spin arising from gluons [2, 3]. This fraction is represented by ΔG, defined as the integral over all Bjorken x of the helicity asymmetry distribution, $\Delta G(x, Q^2)$. Given the capability of accelerating and colliding spin polarized beams at RHIC, made possible by the use of 'Siberian snakes' to preserve the polarization of proton beams in a synchrotron, a new generation of experiments will study the proton spin structure by measuring polarization observables for hard scattering processes initiated by high-energy polarized proton collisions. One of the primary goals of the RHIC spin program is to accurately determine how much of the proton spin results from gluons. Following the completion of the barrel and endcap electromagnetic calorimeters, the STAR detector will provide a world class measurement of the gluon polarization by studying the $\vec{p}\vec{p} \to \gamma + \mathrm{jet} + X$ reaction, using longitudinally polarized proton beams.

The determination of ΔG at STAR will be very demanding. It requires measurement of the spin correlation coefficient, A_{LL}, defined as

$$A_{LL} = \frac{1}{P_{b1}P_{b2}} \frac{\sigma_{++} - \sigma_{+-}}{\sigma_{++} + \sigma_{+-}},$$

with proton beams having longitudinal polarization of magnitude $P_{b1(2)}$. The quantity σ_{++} (σ_{+-}) refers to the normalized γ+jet yield when the proton beams have equal (opposite) longitudinal polarization. For this reaction, leading-order perturbative QCD predicts that A_{LL} is proportional to $\Delta G(x)$. Therefore, the value of A_{LL} that will be measured at RHIC is unknown, because the gluon polarization is unknown. Similarly, most other hard scattering processes will involve gluon scattering at RHIC energies, and hence will also have an uncertain value of A_{LL}. An accurate measurement of A_{LL} requires:

- the careful alignment of the beam polarization vector so that it is either parallel or antiparallel to the momentum vector.
- the determination of the relative luminosity of overlapping proton beam bunches with equal and opposite longitudinal polarizations. Because A_{LL} is a ratio, a determination of the absolute luminosity is not required.
- a determination of the absolute magnitude of the beam polarizations. This measurement will be conducted in a separate experiment studying proton elastic scattering from a polarized proton target.

The first two items in this list must be addressed by the STAR collaboration so that it can achieve its goal of determining ΔG.

The *first measurement* of polarization observables in high energy $\vec{p}\vec{p}$ collisions will be conducted at RHIC during the FY2001 run. Prior experience for such measurements comes from studies of the interactions of polarized proton beams with polarized proton targets, at much lower values of the total energy ($\sqrt{s}$). For those experiments, the relative luminosity determination generally could be accomplished by either counting the beam particles or by monitoring the yield of spin-independent scattering processes initiated by beam-target interactions. At RHIC, the methods for determining the relative luminosity of collisions between beam bunches having different polarization directions must be developed. Following the comissioning of high-energy polarized proton beams, the development of luminosity monitoring techniques is a high priority for the FY2001 run. The completion of this task is facilitated by identifying a high-rate process expected to have a large dependence on the beam polarization.

In traditional lower-energy experiments, verification of the alignment of the beam polarization vector generally relies on measuring parity-allowed, single-spin transverse asymmetries (A_N). The latter observable corresponds to the dependence of the scattered particle yield on the azimuthal angle between the beam polarization and the detected particle. At RHIC energies, the STAR experiment will be unable to observe pp elastic scattering, the only reaction that is known to have (small) non-zero values for A_N. The naive QCD expectation is that A_N will approach zero for particle production at midrapidity. The result is that *some other process*, having a scattering rate dependent on the beam polarization, must be identified to provide the means to experimentally verify that the beam polarization is longitudinal at the STAR collision point.

Special difficulties in polarization measurements at high energies are anticipated because of the very large value of $G\gamma$, specifying the spin dynamics of protons through magnetic fields. The anomalous magnetic moment of the proton is $G = 1.7928$. For a proton beam of energy 100 GeV having its polarization vector in the bend plane of the RHIC rings, there are nearly 200 full revolutions of the polarization vector for every single orbit of the beam. Even very small errors in the magnetic fields, required to guide the proton beams, can result in misalignment of the polarization vector at the point where the beams collide. With both snakes operating in each RHIC ring, the beam polarization vector is perpendicular to the bend plane of the beams. Ultimately, special magnets ('spin rotaters') will be used to precess the proton polarization so that it is longitudinal at the interaction regions (IR) of the STAR and PHENIX detectors, and then restore its direction after the IR. These magnets will be installed *after* the FY2001 run. Following commissioning of the polarized proton beams in FY2001, it is planned to study collisions of longitudinally polarized proton beams at $\sqrt{s}$=200 GeV, by turning off one of the two snake magnets at the top of the ramp to precess the polarization vector into the RHIC bend plane. This will place significant demands on the experiments to verify that the beam polarization is longitudinal. The methods used to verify the direction of the beam polarization for the FY2001 run will remain important for aligning the polarization vectors using the spin rotaters in subsequent years.

Excluding elastic scattering, no measurements of A_N have been conducted for $\vec{p}\vec{p}$ scattering at the collision energies that will be probed at RHIC. Large values of A_N have been measured for leading charged and neutral pions produced at large Feynman x and moderate transverse momentum in $\vec{p}p$ interactions at $\sqrt{s}$=20 GeV. These unexpected results were obtained in a fixed target experiment at FNAL (E704) [5, 6]. A theory explaining this data was developed by Qiu and Sterman [7]. They subsequently extrapolated their QCD-based model to predict comparably large values of A_N for large x_F and small p_T leading pion production at $\sqrt{s}$=200 GeV.

Leading pion production at high energies and small scattering angle is the most likely high-yield process that is sensitive to the beam polarization at RHIC energies. To address the necessary systematic error checks during the FY2001, required to make progress towards the measurement of ΔG, it is important to pursue ways to study pion production at large x_F and small p_T at the STAR IR. Enabling these measurements is the goal of this proposal.

We propose to install a prototype Forward neutral Pion Detector (FPD) in the wide-angle hall (WAH) housing the STAR detector. The prototype FPD will be used to measure the transverse spin asymmetry, A_N, for $\vec{p}p \to \pi^0 + X$ reactions arising from transversely polarized proton beam collisions at the STAR interaction region (IR). Installation of the prototype FPD prior to the polarized proton run, planned for FY2001 RHIC operations, will provide the critical first steps towards the longer term goals of the STAR spin program. In particular, the prototype FPD will provide a crucial test of our ability to measure polarization observables in a collider environment. Furthermore, if A_N is found to be consistent with theoretical expectations, then an experimental method for verifying the direction of the beam polarization vector at the STAR IR is possible.

2 General Aspects of the Proposed Measurement

We propose to measure the parity-allowed transverse single-spin asymmetry, A_N, for leading π^0 meson production at large Feynman-x ($x_F > 0.4$) and small transverse momentum ($p_T \approx$ few GeV/c) produced in the collision of polarized protons at the STAR IR. To a good approximation, $x_F \approx E_\pi/E_{beam}$ and $p_T \approx \theta E_\pi$, where $E_{beam} = 100\,\mathrm{GeV}$ is the energy of one proton beam at RHIC and θ is the polar production angle of the π relative to the beam axis. Hence, to be sensitive to the relevant kinematic range, π^0 detection at small scattering angles ($\theta \approx 30$ mr) is required.

Why is there expected to be a large asymmetry for this process? As previously mentioned, unexpectedly large values of A_N have been observed for pion production in polarized p-p and $\overline{p}$-p high-energy fixed target experiments by the E704 collaboration at FNAL in these kinematics.[5, 6] These values of A_N were 'explained' by J. Qiu and G. Sterman (Reference [7], and references therein), hereafter referred to as QS, as a higher-twist perturbative QCD effect. The QS model was subsequently extended to predict measurable values of A_N for polarized proton collisions at RHIC for pion production at large x_F and small p_T, the results of which can be seen in Figure 1. Qualitatively, the QS model predicts similar results for A_N at both $\sqrt{s}$=20 and 200 GeV.

Some considerations regarding a measurement of A_N at STAR are as follows.

1. The largest asymmetries in the QS model, and observed in E704, are for *charged* pion production. However, $A_N(\pi^+) \approx -A_N(\pi^-)$ at a given x_F and p_T. This means that if the charge of the $\approx 40\,\mathrm{GeV/c}$ pion is not determined (*i.e.*, by a measurement of the bend angle through a known magnetic field), but its energy is measured using a hadronic calorimeter, we would expect to see $A_N(\pi^+ \text{ or } \pi^-) \approx 0$. Therefore, the measurement at STAR should focus on observing high-energy π^0 production.

2. The non-zero value of A_N in the QS model arises from a hard-scattering process. At very small p_T (less than $\approx 1\,\mathrm{GeV/c}$), most of the π^0's are expected to be produced by diffractive processes, not included in the QS model. The value of A_N for these diffractive processes is unknown, but is most likely to be close to zero. Therefore, the measurement at STAR should focus on observing high-energy π^0's with $p_T > 1\,\mathrm{GeV/c}$.

3. The *most probable* opening angle, $\phi_{\gamma\gamma}$, between the two photons resulting from π^0 decay, is given by the *minimum* opening angle, $\sin(\phi_{\gamma\gamma}^{min}/2) = M_\pi/E_\pi$. For a 40 GeV π^0, this is an angle of $\approx 7\,\mathrm{mr}$. This results in the most probable separation between the two photons equal to 5 cm at a detector that is 750 cm distant from the IR. Therefore, calorimeter bars of reasonable dimensions will not be able to separate the showers produced by the two photons.

4. If only one of the two photons arising from π^0 decay were detected, then x_F and p_T for the π^0 would not be measured. The energy of a single photon from π^0 decay has equal probability to

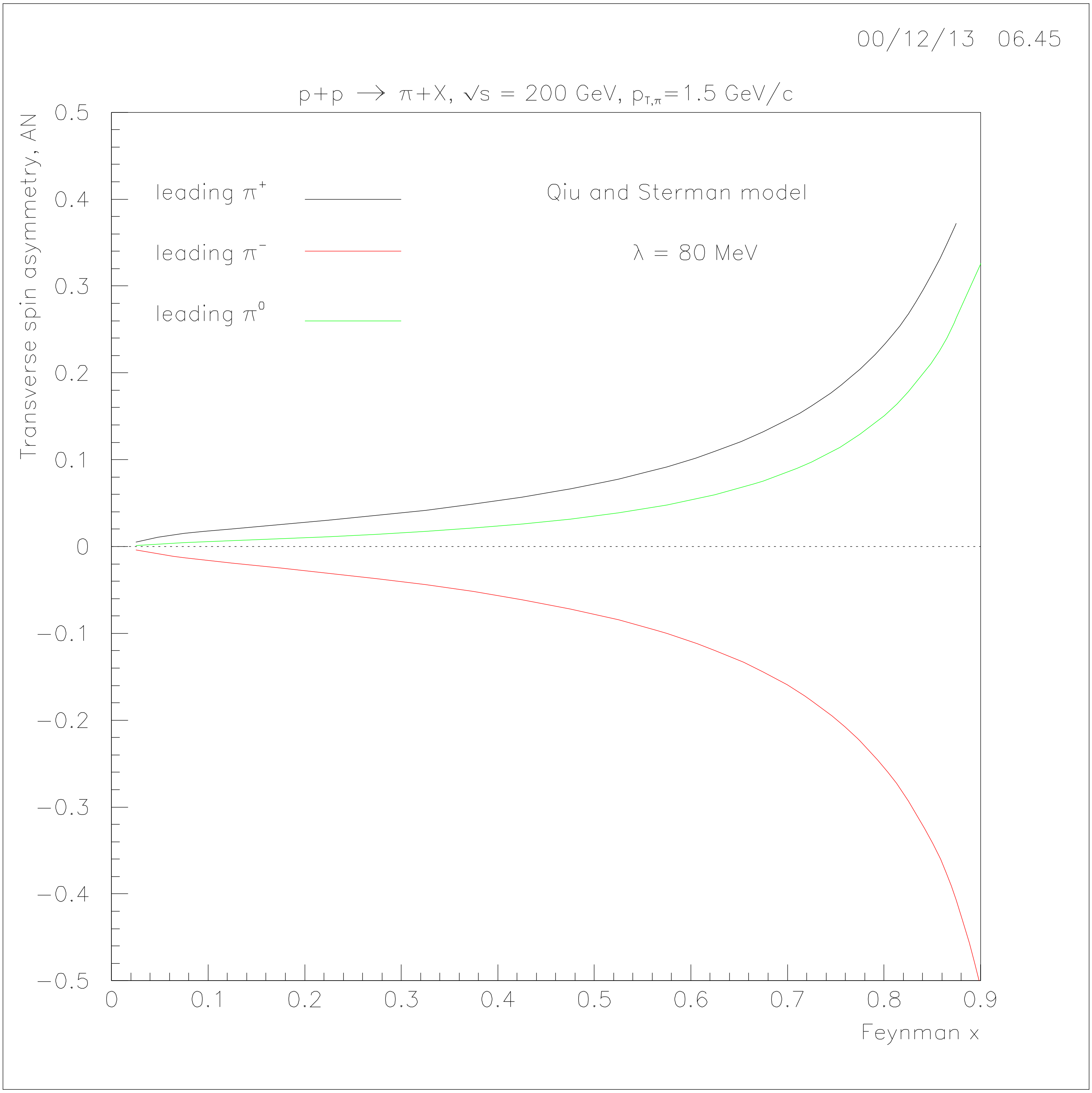

Figure 1: Prediction of the transverse single-spin asymmetry, A_N, from the model of Qiu and Sterman[7], evaluated at the kinematics for the proposed detector at STAR. The magnitude of the twist-3 contribution to the hard scattering amplitude is set by the λ parameter, and was chosen in Reference [7] to give a rough match to the FNAL E704 data.

have any value between ≈ 0 and $\approx E_\pi$. In other words, there are no 'simple expectations' for A_N for an inclusive photon production measurement (photons arising primarily from the decay of a π^0 or η^0 meson). One would have to rely on a sophisticated Monte Carlo simulation of the detector acceptance, accounting for all sources of large energy deposition in the calorimeter and including all of the material between the IR and the detector, to establish the 'expected' value for A_N for inclusive photon production. Therefore, a measurement capable of *identifying* energetic π^0 is very desireable.

5. A positive indication that a leading π^0 has been produced is possible by reconstructing the invariant mass of a pair of photons. As discussed in Section 5, good resolution for the $\gamma\gamma$ invariant mass can be obtained by making a *good measurement* of the opening angle between the two decay photons, and only a *crude measurement* of the individual photon energies.

6. Any measurement in the forward direction would probably need to be able to distinguish between (possibly sizable) background processes and the photon pairs which arise from the decay of π^0 mesons produced by a *p*-*p* collision at the IR.

Concerning this last point, there are many possible sources of background expected in the forward direction. This background could result from 'beam-gas' events, where protons are scattered from gas molecules that linger in the beam pipe in spite of our best pumping efforts. There could also be small-angle elastic or diffractive proton scattering, followed by interactions of the scattered proton with matter surrounding the IR. A third possible source of background is protons in the halo of the beam which "scrape" flanges on the beam pipe (for example) and shower in the forward direction. The absolute and relative amounts of each of these sources of background, and their effects on the proposed π^0 A_N measurement in the new RHIC *p*-*p* collision environment, is essentially unknown.

Positive identification of *pp* collisions can be accomplished by reconstruction of an event vertex, based on midrapidity charged particles tracked by the STAR time projection chamber (TPC). A standard event generator (PYTHIA) indicates that most of the hard-scattering events producing a large x_F, small p_T π^0 also produce 'soft', *i.e.*, low p_T, charged hadrons at midrapidity ($|\eta| < 1.5$), as can be seen in Figure 2. These charged hadrons arise from the hadronization of 'spectator partons' following the *pp* collision. They can be tracked by the TPC, and their vertex along the beam, most likely to be near $z \approx 0$, can be reconstructed. 'Beam-gas' events will most likely produce an event vertex at much large $|z|$ and so can be distinguished from *pp* collision events. To achieve the discrimination between FPD events arising from *pp* collisions versus those arising from background, it is important that the prototype FPD be able to obtain *correlated information*, on an event-by-event basis, from the STAR TPC. In an identical way, the TPC could be used to help reduce the contamination from background produced by small angle elastic or diffractive scattering, followed by a secondary interaction with the material in the vicinity of the IR. Small-angle elastic and diffractive

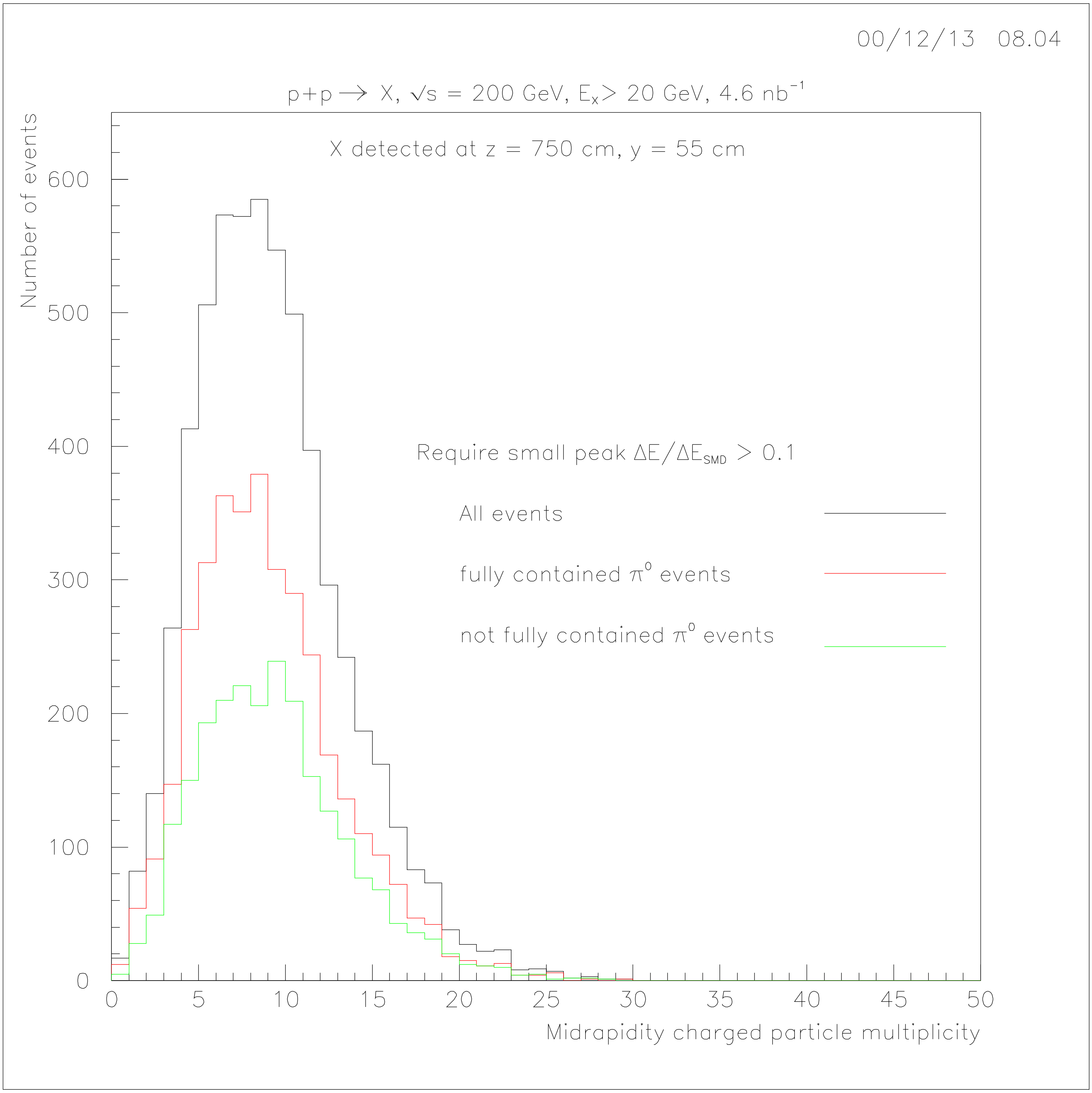

Figure 2: A PYTHIA simulation of the multiplicity distribution of charged particles with $|\eta| < 1.5$ (*i.e.*, in the nominal STAR TPC acceptance) for events which also deposit greater than 20 GeV in the pEEMC at the proposed location of the prototype FPD. Tracking done with the STAR TPC could be used to pinpoint the event vertex to help beat down the background expected at the prototype FPD. Details of the analysis will be given in Section 5.

scattering will not produce significant charged particle multiplicity in the central region ($|\eta| < 1.5$).

To enable us to correlate data from the FPD with charged particle tracks near midrapidity, it is necessary to trigger the STAR TPC when there is large energy deposition in the FPD. As well, a link between the event data from the FPD and from STAR must be established. There are other subsystems within STAR which have comparable trigger and data acquisition (DAQ) interfaces to STAR, such as the Zero-Degree Calorimeter and the RICH detectors. We propose to use analogous interfaces between the prototype FPD and STAR. The standalone DAQ for the prototype FPD will be described in Section 6, and the interface to the STAR Trigger and DAQ will be discussed in more detail in Section 8.

3 Some Details of the Proposed Measurement

We propose to mount forward electromagnetic calorimeters on the 'tunnel platform extension' in the STAR wide angle hall (WAH). There is some space available on the east side of STAR, with a clear view of the IR, that is, with less than 1 radiation length of intervening material (see Section 5). The detectors would be mounted at a z coordinate of $\approx 750\,\mathrm{cm}$ and radial distance of $\approx 50\,\mathrm{cm}$ from the beam.

Two types of detectors are being considered:

1. A Pb/plastic scintillator sampling calorimeter, including a prototype scintillator strip 'shower maximum detector' (pSMD). Hereafter, this detector will be referred to as the pEEMC, the acronym standing for the 'prototype endcap electromagnetic calorimeter'. This detector is being considered for several reasons:

   - The small spacing of the scintillator strips of the pSMD will allow a *good measurement* of the opening angle between the two photons arising from π^0 decay. From the known detector position, the distance between the peak centroids from the pSMD x and y planes precisely determines the distance between the two photons at the pEEMC, and hence the opening angle between the two photons.
   - The detector provides a good measurement of the total energy deposited by the pair of photons, for fully contained showers. The energy resolution of the pEEMC towers is expected to be $\sim 17\%/\sqrt{E}$, meaning that both x_F and p_T for the π^0 will be well measured.
   - The detector provides a *coarse measurement* of the individual energies of the two photons arising from π^0 decay. The energy deposited in the pSMD plane by each photon is used to subdivide the total energy measured in the pEEMC sampling calorimeter, to provide a crude determination of each photon's energy. With this information, and the opening angle measurement, the $\gamma\gamma$ invariant mass can be reconstructed with good resolution, as further discussed in Section 5.

- This detector has been tested in a high-energy electron beam at SLAC, and performs as expected. Further testing of this detector is planned in a January, 2001 test beam at SLAC.

It is imagined that the pEEMC would be mounted on the north side of the 'tunnel platform extension' in the STAR WAH. This will provide a single arm that could be used to measure the π^0 production asymmetry for beam bunches with spin up and spin down. Such a measurement will severely test our ability to determine the relative luminosity of the collisions of spin up and spin down beam bunches in RHIC. The expected beam polarization for the FY2001 polarized proton run at RHIC is 50% and the magnitude of A_N is expected to be 0.05. Hence, relative luminosity monitoring, accurate to much better than 2.5% is required. This requirement is far less demanding than is needed for the A_{LL} measurement that will determine ΔG, and is an essential first step towards that longer term goal.

2. There is only one detector of the type described above. Building additional detectors of this type, or of a type that is best suited to the polarized *p*-*p* collision measurements next summer, is not feasible in the available time. There do exist Pb-glass detectors that could be available for positioning on the south side of the beam, and above and below the beam. These detectors would not be able to identify π^0's, but would measure inclusive photon production. Coarse transverse segmentation could be used to ensure that showers are contained within the Pb-glass detectors. With the understanding of the data-collection environment that is expected to be gained from use of the pEEMC, it is envisioned to use the inclusive photon asymmetry measured with the Pb-glass counter on the south side of the beam pipe as a systematic check on the asymmetry measured with the pEEMC. The counters above and below the beampipe then could be used to measure a *transverse* asymmetry during *longitudinal* *p*-*p* running, as a check for transverse components of a longitudinally polarized beam.

4 Technical Description

There exists a tunnel platform extension at $z \approx 7-8\,\mathrm{m}$ on the east side of the STAR detector where we propose to put the pEEMC and the Pb-glass detector arrays, together called the Forward π^0 Detector (FPD). The tunnel platform extension extends from the tunnel into the WAH at the height of the tunnel floor. Rigidly attached to the platform extension is a beam-pipe support structure at $z \approx 8\,\mathrm{m}$. The orientation of this tunnel platform extension is asymmetric with respect to the beam pipe, with more room available on the north side of the beam pipe than on the south side of the beam pipe. We propose to put the FPD in front of the beam-pipe support structure on the east side of the IR, at $z \approx 7.5\,\mathrm{m}$, at a transverse distance of $\approx 30\,\mathrm{cm}$ on the north side of the beam pipe at beam height. A drawing of the tunnel platform extension can be seen in Figure 3. It is essential

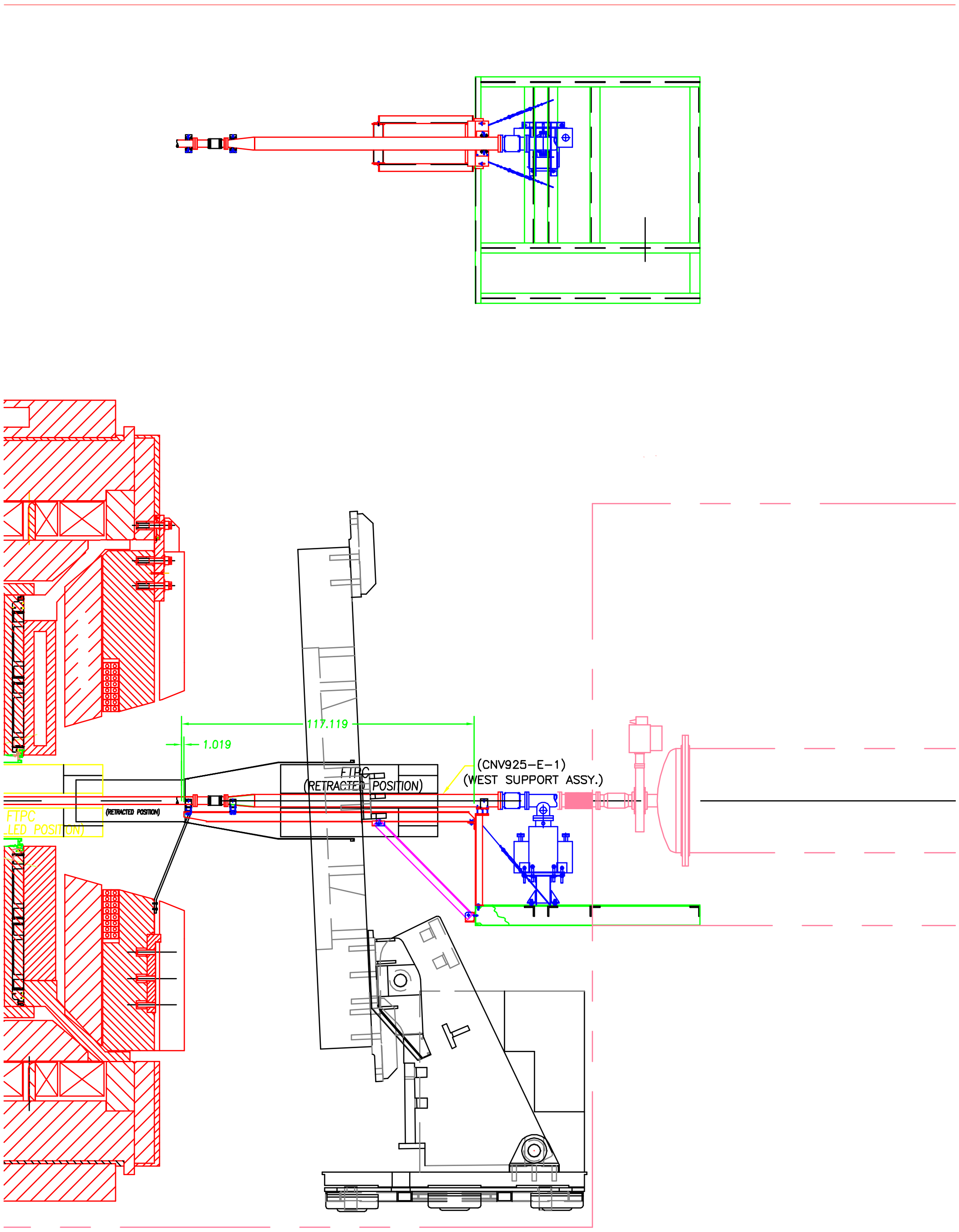

Figure 3: Drawing of the west tunnel platform extension. Note that we actually propose to install the FPD on the east tunnel platform extension. The upper figure is the top view, while the lower figure is the side view.

that the FPD has a relatively unobstructed view of the STAR IR. GSTAR estimates of the material between the IR and this proposed location for the FPD are discussed in Section 5.

The width of the active region of the pEEMC is $\approx$ 32 cm. The center of the calorimeter will be located at a transverse distance of $\approx$ 26 cm from the center of the beam pipe, limited first by the minimum bend radius necessary for the clear fiber optical connections located on the side of this prototype box, so that the active region covers the angular region $\approx 25-85$ mrad. Thus, for a 40 GeV π^0 at $z = 7.5$ m, the active region of the pEEMC spans approximately the range $1.0 < p_T < 3.4$ GeV.

The pEEMC is a traditional Pb sampling calorimeter with a sampling fraction of $\approx 6.5\%$, arranged in a configuration similar to an early design of the STAR endcap EMC. The detector is comprised of 24 layers of 5 mm thick Vulcan lead sheets interleaved with 24 layers of 4 mm thick Kururay SCSN-81 plastic scintillator sheets, presently beginning with a lead converter layer to simulate material upstream of the detector stack, for a total of approximately 21 radiation lengths. The view of the interleaving arrangement as seen from the top of the prototype box can be seen as a photograph in Figure 4, and is schematically shown in Figure 5. The scintillator sheets within the calorimeter have been machined into "megatiles". Optical isolation grooves were machined into a single scintillator layer, which were then filled with titanium-dioxide loaded epoxy. Following the curing of the epoxy, "sigma grooves" were machined into the scintillator to allow the insertion of 0.83 mm-diameter (Y11 doped) wavelength shifting (WLS) optical fibers, produced by Kururay. Each layer has 12 tiles machined into it, in a 3×4 pattern resembling the inner radius of an early design of the STAR endcap EMC, and is schematically shown in Figure 5. The 24 scintillation sheets are thereby divided into 12 projective towers.

The first two scintillator layers are preshower layers, different from the rest of the scintillator layers in that the response of each preshower tile is read out individually. A second WLS fiber is inserted into the sigma grooves of each tile in the preshower layers to collect and transport scintillation light to tower photomultiplier tubes, discussed below. The preshower scintillator layers are each 5 mm in thickness.

Following the sixth Pb layer, two planes of finely segmented scintillator strips are used as a shower-maximum detector (SMD). The SMD detector is designed primarily to aid in resolving the two close-lying photon showers characterizing π^0 decay. The original prototype SMD is made of triangular scintillator strips, extruded from polystyrene pellets doped with flourescents. The strips each have a transverse profile approximating an equilateral triangle with an apex-to-base height of 5 mm. A hole running axially along the center of each triangle allows the insertion of a 0.83 mm WLS fiber which is used to collect and transport the scintillation light. Individual triangular strips are wrapped with 50 μm of aluminized mylar to optically isolate them from their neighbors. The wrapped scintillator strips were then epoxied between two G-10 sheets to form two planes, oriented into orthogonal y and x planes. There are 100 strips running in the horizontal direction and 60 strips

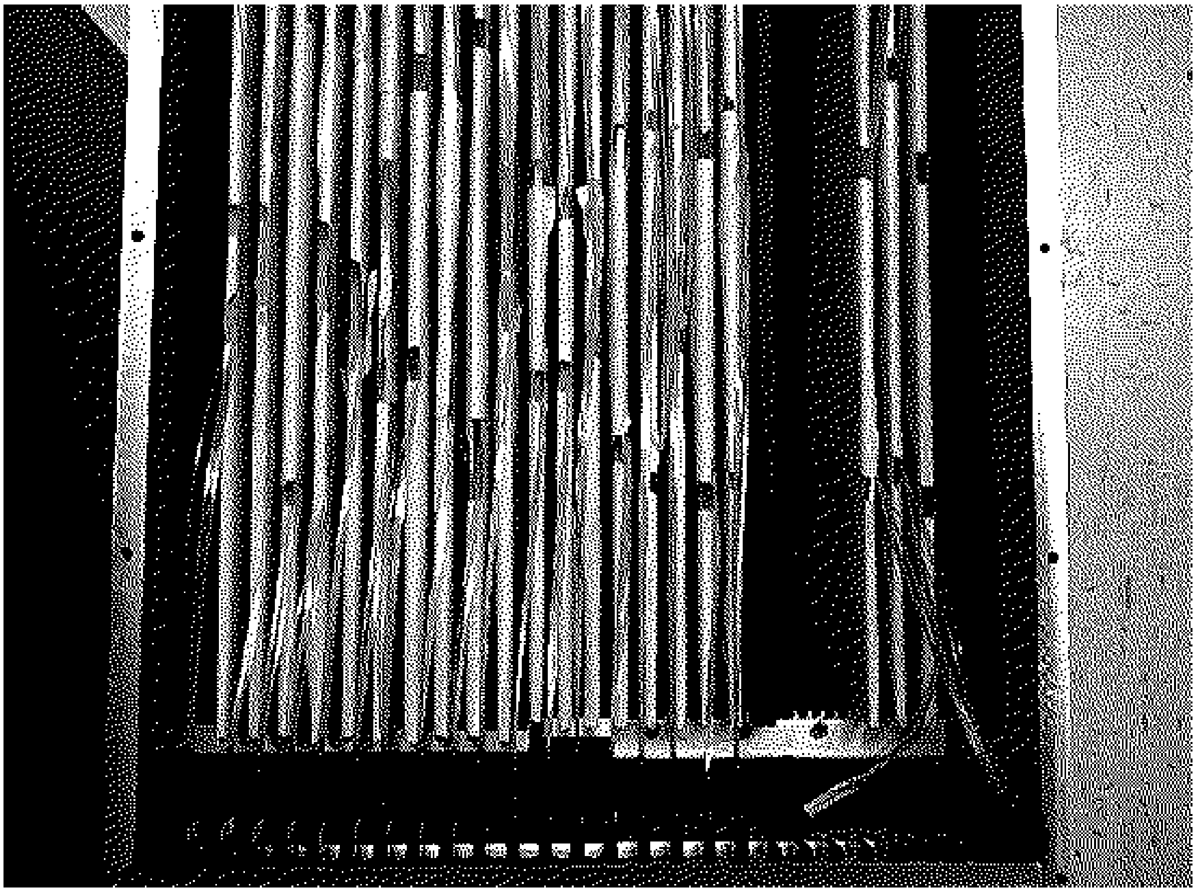

Figure 4: Photograph of the Al prototype box from above, with the top cover plate removed. In this picture, the photons are incident from the right. Note that the Pb sheets are not inserted, and the third through sixth layer of scintillator sheets have been removed to ease the insertion of pSMD planes.

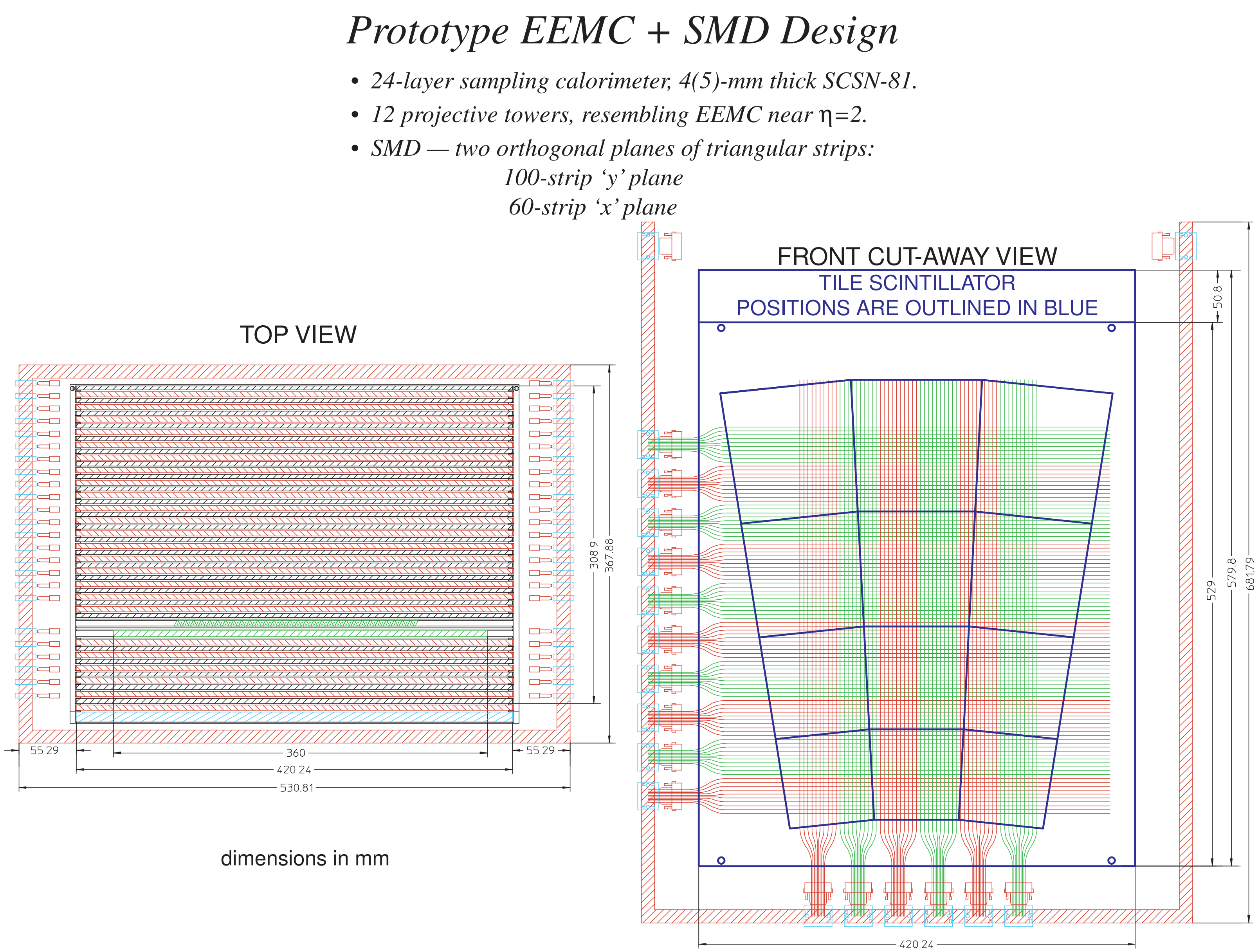

Figure 5: Schematic drawing of the pEEMC and pSMD.

in the vertical direction, giving transverse shower profiles in the y- and x-directions, respectively. The decay of an 60 GeV π^0 will result in a most probable distance between the two photons of 34 mm at the proposed location of the FPD, producing the worst case centroid separation on the pSMD x- and y-planes of $34/\sqrt{2} = 24\,\mathrm{mm}$, which is a difference of about 8 strips.

Most recently, scintillator strips having triangular profiles of 10 mm (base) $\times$ 7 mm (height) were extruded, to allow the production of the SMD planes of the STAR endcap EMC. A second set of pSMD planes was constructed to permit an in-beam test at SLAC, scheduled for January, 2001. To date, pFPD simulations have only been performed for the originl pSMD planes, with the smaller triangular strips. It is likely that the coarser pitch of the new pSMD will still permit π^0 reconstruction over a broad range of energies. This will be confirmed using similar simulations to those described in Section 5.

The calorimeter is contained within a light-tight Al box of dimensions $15'' \times 21'' \times 28''$ $(l \times w \times h)$. A photo of the already existing prototype box can be seen in Figure 6. With the Pb sheets inserted into the prototype box, the total weight of the box is $\approx 1100\,\mathrm{lbs}$. Without the Pb sheets, as is seen in Figure 4, the box is $\approx 130\,\mathrm{lbs}$. Four steel O-ring brackets are bolted to the sides of the box to facilitate transportation and for earthquake safety rigging, that was required for running at SLAC. In its final configuration, the prototype box will be laid on its right side on a table *i.e.*, on the side without the connectors for the y pSMD layer, with the x pSMD layer connectors next to the beam pipe. Since the towers are projective, the prototype box will be oriented at an angle on this table so that the π^0 decay products will be incident more normally on the towers. The four legs which extend from the bottom of the prototype box, seen in Figure 6 will be removed.

WLS fibers (all $< 0.5\,\mathrm{m}$ in length) transport the scintillation light from the pSMD strips to optical connectors located in the wall of the Al prototype box. The optical connector at the wall of the Al prototype box is a 10-fiber connector produced by DDK Electronics. There are a total of 16 of these 10-fiber connectors, six of them located along the bottom of the prototype box and 10 of them located along the left side of the box, as shown in Figure 5. With these connectors, a one-to-one connection is made between the WLS fibers and 0.91 mm-diameter clear fibers prepared by a group from Michigan State University. The 16 wrapped bundles of 10 clear 0.91 mm fibers for the pSMD signals transport light to a second Al box, called the MAPMT box. Each bundle is fed through one of 16 feedthroughs (two rows of eight feedthroughs) on the MAPMT box.

We plan to locate the MAPMT box on the tunnel platform extension. The MAPMT box is $26'' \times 19'' \times 8''$, and weighs $< 25\,\mathrm{lbs}$. There are handles on the sides of the MAPMT box to facilitate transportation. The box can hold up to 12 MAPMT's in total, and has SHV connectors mounted on the back. The back end of the MAPMT box is open to the air. The MAPMT box contains 12 Hamamatsu 6568 multi-anode photomultiplier tubes (MAPMT's), with 16 pixels each. The clear fibers are coupled directly to pixels on the MAPMT's, one SMD strip per pixel, and are routed

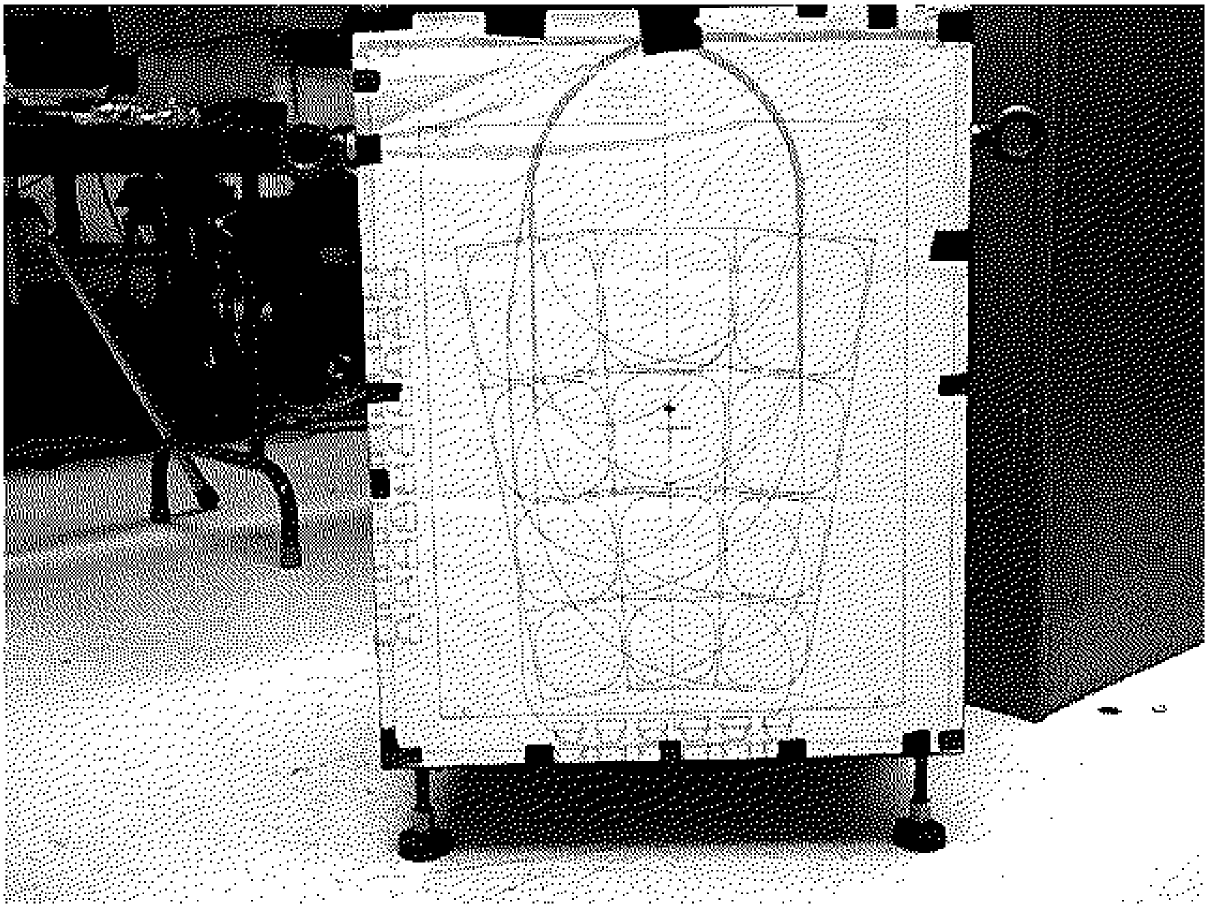

Figure 6: A photograph of the Al prototype box, as seen from the front. A 1:1 scale drawing of the megatile, showing the isolation grooves, the sigma grooves, and the fiber routing layer, has been taped to the box. From this drawing we can see that the WLS fibers for the towers go to connectors on the top left and top right of the box, while the WLS fibers for the pSMD layers go to the left and bottom edges of the box for the y and x pSMD layers, respectively. This box will be laid on a table on its right side when it is installed at RHIC.

within the MAPMT box in such a way to minimize crosstalk between adjacent strips. The bases of the MAPMT's are resistive voltage dividers manufactured by Hamamatsu, modified to be tapered for better linearity, and are biased to $< |1200|$ V. For the STAR endcap EMC, Cockcroft-Walton (CW) bases will be used. A single prototype exists at present. Equipping all of the MAPMT with CW bases for running at STAR may be possible, thereby eliminating the need for high voltage. The details of the existing HV connections and safety considerations thereto will be discussed in Section 7.

The sixteen anode outputs from each MAPMT are sent through passive delay line chips, and the currents are subsequently transported to a LeCroy 4300B analog-to-digital converter (FERA) over shielded twisted pair cables. The CAMAC crate for the FERA modules would be located directly below the tunnel platform extension, *i.e.* on the floor of the WAH. The CAMAC crate, and associated trigger electronics, is mounted in an electronics rack containing a 208 V isolation transformer capable of supplying 5.25 kVA of AC power. Both 208 V AC power and an ethernet connection is required for the electronics.

The scintillation signals from the towers are handled in a different way than those from the SMD, and uses the scheme which is foreseen to be used for the STAR endcap EMC towers. As mentioned before, the scintillation light which is induced in each tile by a shower is collected in WLS fibers for transport to the edge of the Al prototype box. The lengths of WLS fibers used for the towers changes, depending both on the size of the sigma grooves and on the route used to arrive at the edge of the prototype box, and ranges from 930 to 1600 mm. The 12 WLS fibers originating from a single layer in each of the 12 towers are bunched into two 10-fiber optical connectors—six tiles per 10-fiber connector, for a total of $12 \times 24/6 = 48$ 10-fiber connectors on the prototype box for the towers. From the optical connectors on the side of the Al prototype box, the signals from the tiles are transported via 0.9 mm-diameter clear fibers to optical connectors on the side of a separate Al box, which is called the tower PMT box. The 48 clear fiber bundles, bundled in groups of six, are all ≈ 10 ft. long.

The photomultiplier tubes for the tower signals are housed in the tower PMT box, planned to be located on the tower platform extension together with the MAPMT box. The tower PMT box is $28'' \times 28'' \times 13''$, and weighs < 25 lbs. There are Al handles on the sides of the Tower PMT box to facilitate its transportation. On the front of the Tower PMT box are optical connectors to go from 0.9 mm- to 1.0 mm-diameter clear fibers. The scintillation light from all of the layers within a single tower are summed together by routing all of the 1.0 mm fibers from a given tower (one from each pair of connectors) onto a lucite light mixer that is viewed by the photocathode of a single EMI 9107B PMT (12 total). On the back of the Tower PMT box are feedthroughs for LEMO cables for the analog signals from the 12 Tower PMT's. The bias voltage is supplied to the tower PMT using Cockcroft-Walton bases described in Section 7.

The 12 signals from the 12 tower PMT's are delayed ≈ 150 ns by using ≈ 100 ft. of coaxial cable

(Belden RG-58A/U with LEMO connectors Kings Electronics 1075-8). The signals are then fed into a LeCroy 4300B FERA module. The FERA module for the Tower signals will be housed in the same CAMAC crate as the FERA modules for the pSMD, located on the floor of the WAH.

In addition to the prototype EEMC detector, we propose to install three sets of counters above, below, and south of the beam pipe. Each of these counters will be comprised of four Pb-glass detectors, with the idea to use the information from all four detectors simultaneously to see how well the electromagnetic shower is contained within the Pb-glass. The dimensions of each Pb-glass detector, including the phototube and base, is approximately $25'' \times 2.5'' \times 2.5''$, with a weight of 16.8 lbs, so that four of them together would be approximately $25'' \times 5'' \times 5''$ and weigh ≈ 67 lbs. The Pb-glass detectors we expect to use, including the photomultiplier tubes and resistive bases, have come from Argonne National Lab, and we plan to borrow them from an experiment for which they are currently being used at IUCF.

5 Monte Carlo Simulations of pEEMC Performance

Minimum bias events were generated by PYTHIA for pp collisions at $\sqrt{s} = 200\,\mathrm{GeV}$, including hard parton scattering, 'soft' pQCD processes, and diffractive processes. To date, statistics for only $4.6\,\mathrm{nb}^{-1}$ of integrated luminosity have been generated, corresponding to ≈ 1000 seconds of collisions at a luminosity of $5 \times 10^{30}\,\mathrm{cm}^{-2}\mathrm{s}^{-1}$. In 1000 s of collisions at this luminosity, this results in ≈ 2500 π^0 events which are reconstructed, following a procedure described below.

Showers in the pEEMC were simulated by a detailed GEANT model of the detector. That same model has been compared to shower profiles measured by the pSMD during an in-beam test of the detector at SLAC using 5,10 and 20 GeV electrons. For the π^0 analysis, simulated events were chosen by demanding an energy deposition of at least 1.3 GeV in the calorimeter towers, corresponding to the energy deposited by an incident 20 GeV electron. The simulated response of the SMD was used to identify events which most likely had a pair of photons within the fiducial volume. An algorithm, similar to what is envisioned for the analysis of data that would be obtained at STAR, was applied to the GEANT simulations to identify and analyze events with peak pairs in the pSMD planes. The output from this analysis for a single event containing an energetic π^0 whose daughter photons are fully contained within the detector, is shown in Figure 7. The two peaks are fit with functions that adequately describe the average transverse shower profile, with shape parameters that freely vary to account for event-to-event fluctuations. The positions of the centroids of the two fits can be related to the opening angle between the two photons. The relative area underneath the two peaks can be used to (roughly) subdivide the total shower energy between the two photons. A cut is placed on the pulse height of the smaller pSMD peak, requiring it to be $> 10\%$ of the total energy deposited in the pSMD plane. This condition effectively eliminates events induced by single photons, corresponding to the primary background expected in the detector from pp collisions. This condition has no effect

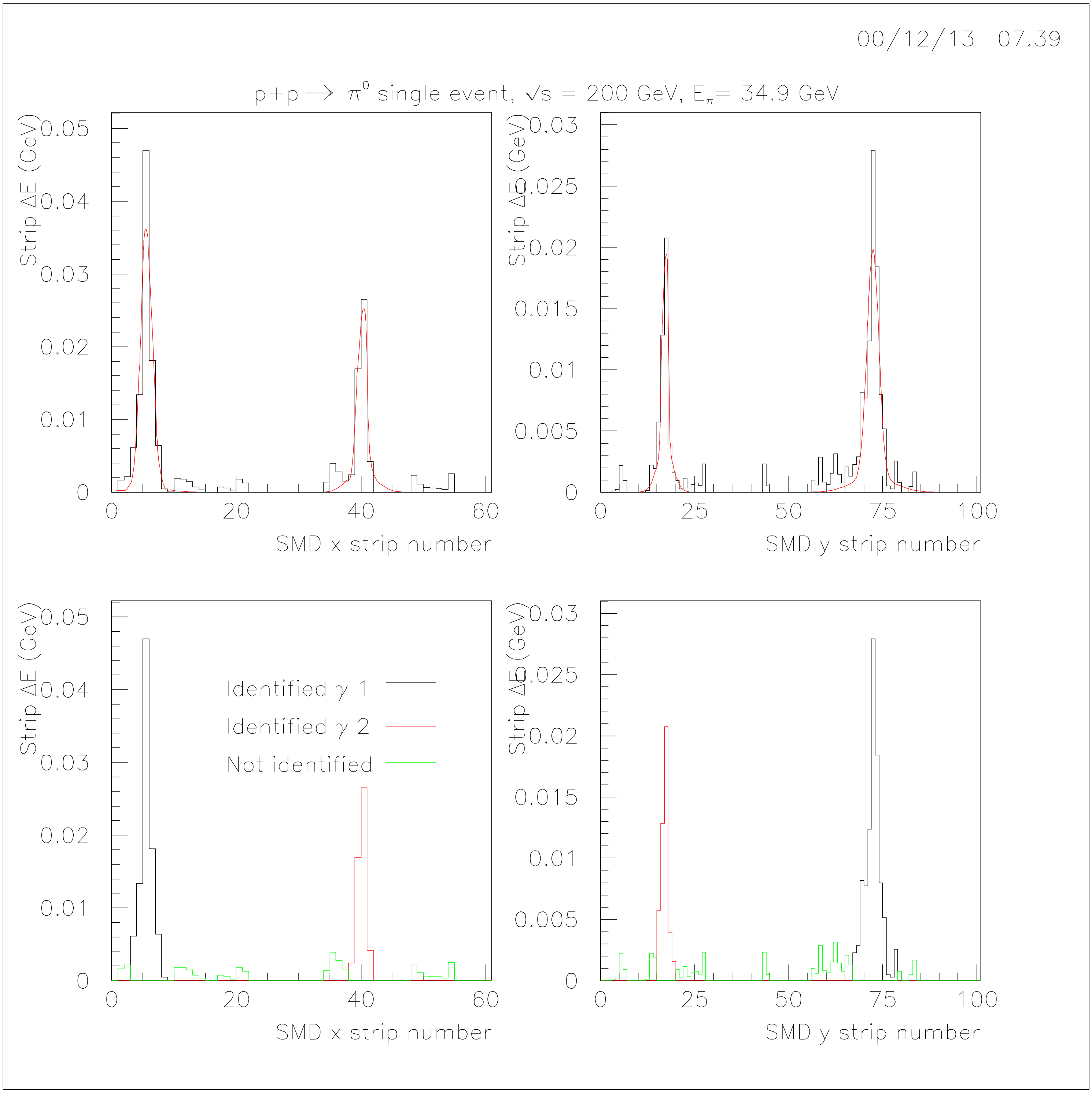

Figure 7: GEANT simulation of the energy deposited in the x and y pSMD planes as a function of pSMD strip position for a single event containing an energetic π^0, with its daughter photons completely contained within the detector acceptance. The two peaks are fit with a function that describes the average SMD profile in the upper plot. Similar fits are performed for all events. The centroids of the peaks can be related to the opening angle between the photons. The relative area underneath the two peaks can be used to (roughly) subdivide the total tower energy between the two photons.

on determining the energy of the π^0. It corresponds to selecting $\pi^0 \to \gamma\gamma$ decays, where the two photons equally share the π^0 energy. Hence, reconstruction efficiency is lost so as to gain a powerful means of suppressing background.

A significant peak in the $\gamma\gamma$ invariant mass is observed and can be seen in Figure 8, with only a small background from events not arising from $\pi^0 \to \gamma\gamma$, when including the condition that the peaks found in the analysis of the SMD response each have at least 10% of the energy deposited in the pSMD plane. At present, $\sim 40\%$ of all triggers result in a reconstructed π^0 event. The conspicuous suppression of η mesons arises because the opening angle between the two photons produced by the $\eta \to \gamma\gamma$ decay branch (representing 39% of all decays) is larger than the detector acceptance, except for the highest energy η mesons, which are not abundantly produced.

Another result from the MC simulation is that x_F for the π^0 is well measured due to the containment of the electromagnetic showers from the two photons. The relative difference between the simulated and reconstructed x_F is 2% at E_π=40 GeV, consistent with the expected energy resolution of the calorimeter towers. The energy distribution for reconstructed events, for both the π^0 signal and the background, is shown in Figure 9. As just mentioned, the rapid falloff of the event rate with increasing pion energy (or x_F) is evident from this distribution.

Another result from the simulation is that p_T for the π^0 is well measured due to the fine segmentation, *i.e.*, position resolution, of the pSMD. The difference between the simulated and reconstructed p_T is 4.8%, consistent with the expected position resolution of the shower centroids. At present, the reconstructed p_T does not rely on a reconstructed collision vertex, accounting for approximately half of the finite p_T resolution. The p_T distribution for π^0 events reconstructed by the pEEMC can be seen in Figure 10. The rapid falloff of the event rate with increasing p_T is evident from this distribution.

It is important that the line of sight from the target to the FPD be relatively clear of obstructions in order to reduce the rate of background showers at the FPD. To better understand the amount of material along the line of sight, we use "Geantino's" in a full GSTAR simulation (version `SL00M`) to probe from the nominal interaction point ($z = 0$ and $r = 0$) to the planned position of the FPD. For this study, we use the geometry file for year 2a, which includes the FTPC, the pVPD, the beampipe, and the beampipe flanges. The number of radiation lengths is plotted versus η in Figure 11. The large peak at $\eta > 5$ is due to the beampipe transition located at $z \approx 4\,\mathrm{m}$, which connects the 3" O. D. beampipe running through STAR to the 5" O. D. beampipe used for the rest of RHIC. The amount of material seen at the FPD by particles coming from the STAR IR is typically < 1 radiation length. Note that neither the shape nor the magnitude of the radiation length distribution changes as we move from $z = 6.5\,\mathrm{m}$ to $z = 7.5\,\mathrm{m}$.

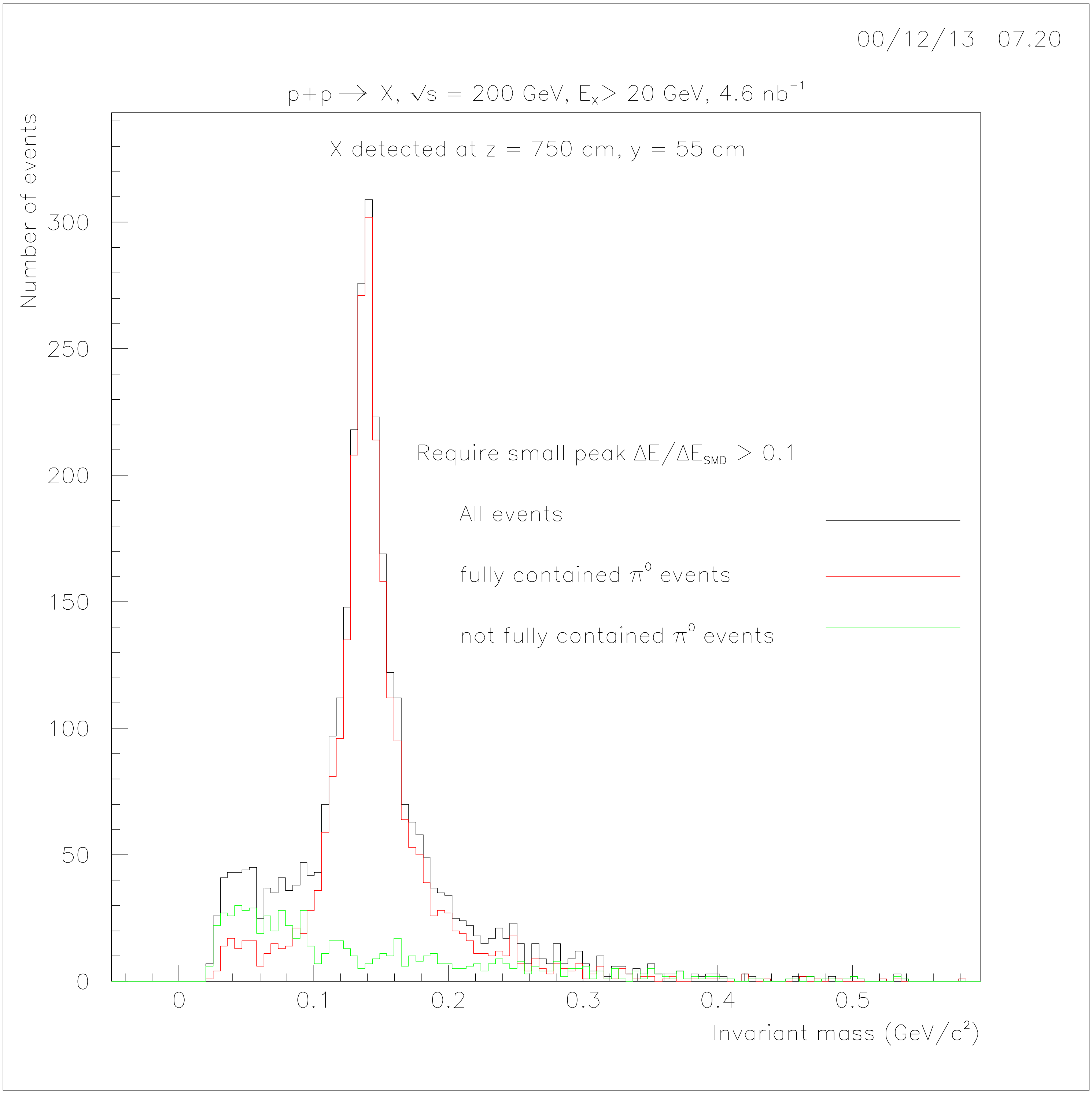

Figure 8: The di-photon invariant mass spectrum reconstructed from GEANT events simulating the expected response of the pEEMC and pSMD. The π^0 peak is clearly visible in this distribution. The "background" is from events whose electromagnetic showers are not fully contained within the pEEMC volume.

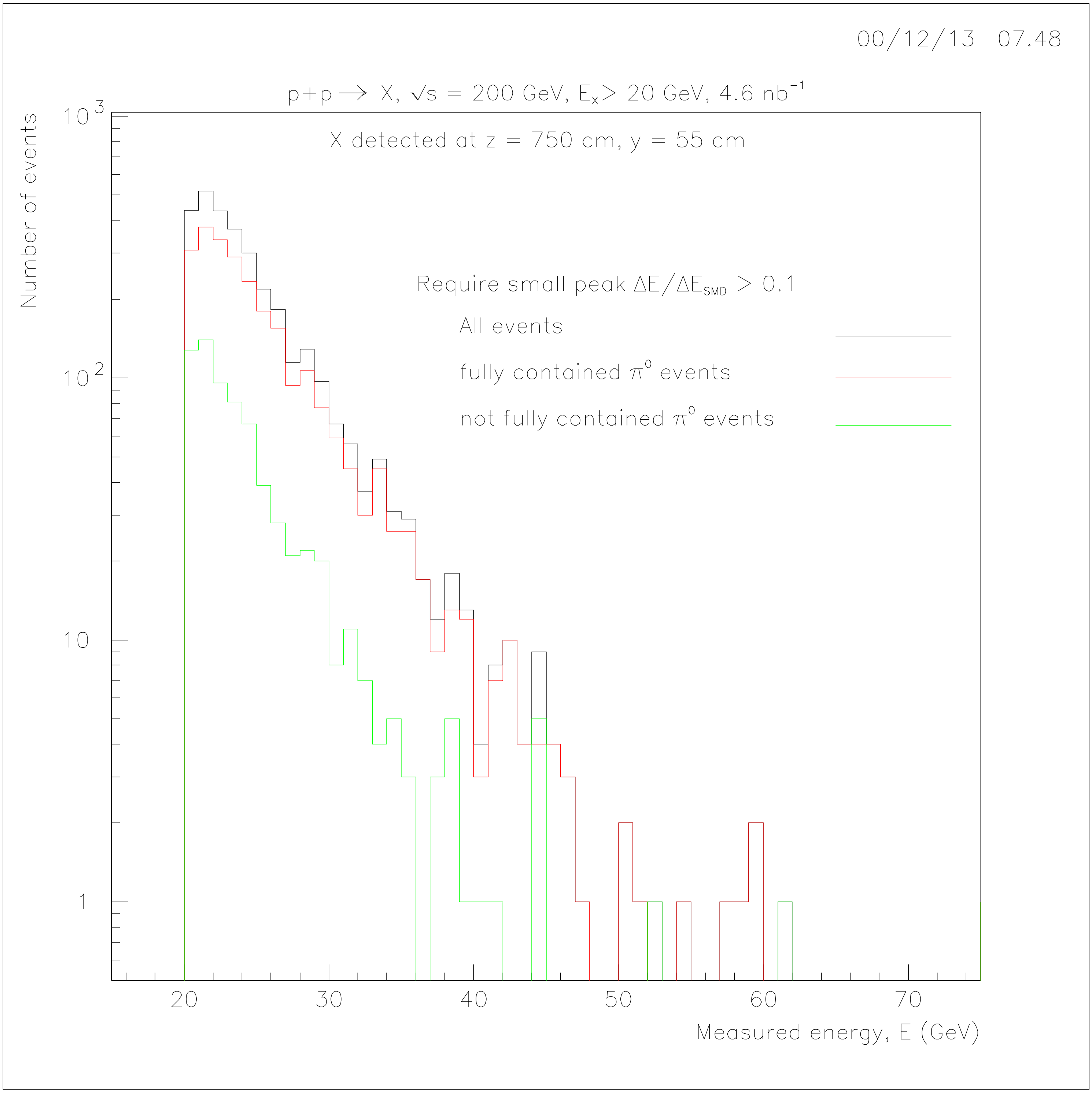

Figure 9: Energy spectrum as reconstructed from GEANT simulations of the energy response of the pEEMC. Note the steep falloff of the event frequency as a function of E_π.

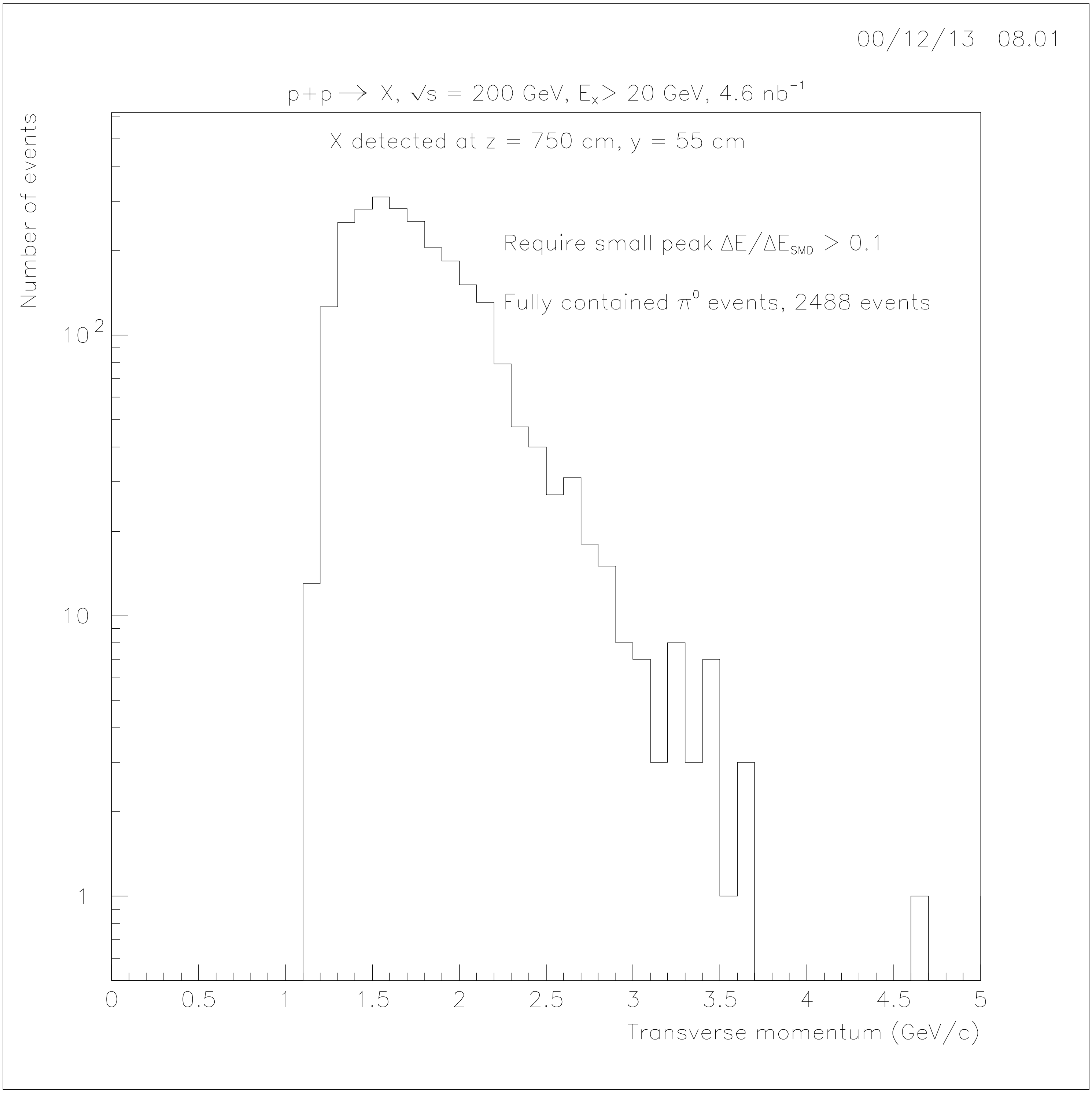

Figure 10: MC simulation of the transverse momentum distribution of π^0 mesons for events whose energies are contained fully within the pEEMC. The distribution is peaked strongly in the forward direction.

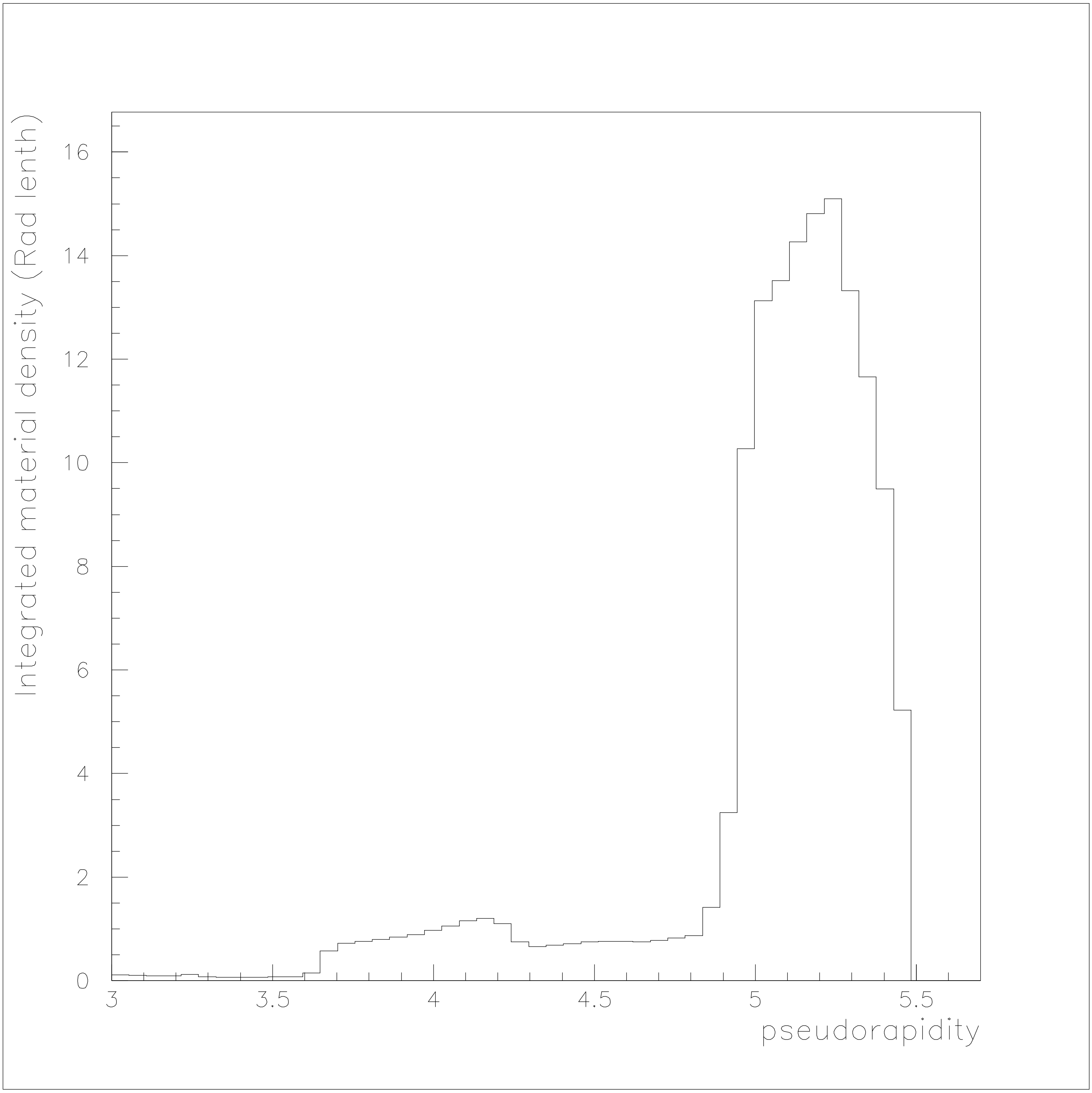

Figure 11: The radiation length plotted versus pseudorapidity, η, integrated over the range $0 < \phi < 1$ radians, at $z = 7.5\,\mathrm{m}$. The proposed location of the FPD approximately covers the range $3.3 < \eta < 4.3$. The large peak at $\eta > 5$ is due primarily to the beampipe transition at $z \approx 4\,\mathrm{m}$.

Table 1: Table of requirements for the STAR endcap EMC Tower PMT's.

Item	Description of parameter	Parameter value
1	PMT size	≤ 30 mm diam; photocathode active area > 20 mm
2	PMT maximum length	115 mm
3	Dynode structure	10 or 11 stages, *linear focused*
4	Photocathode	Bialkali, with QE $\geq 15\%$ @ 490 nm; Nonuniformity $< \pm 20\%$ over active area
5	Electrostatic shielding	Dagged and sleeved (HA coating)
6	Socket	Socket must be included
7	Maximum anode to cathode HV	-1500 V DC
8	Rise time	≤ 5 ns
9	Optimum gain	$> 2 \times 10^5$ for all PMT's within $\Delta V = \pm 100$ V
10	Pulse nonlinearity	$\leq \pm 2\%$ for I_{peak} between 0-50 mA @ gain $= 2 \times 10^5$
11	Dark current	< 1 nA @ gain $= 2 \times 10^5$
12	Magnetic field sensitivity	$< 50\%$ gain reduction in 1.0 G field transverse to PMT axis
13	PMT aging	$< 50\%$ gain reduction after 10-year exposure to total integrated charge of 25 C
14	Long term instability (100 day period)	$< 2\%$ gain variation after initial 25-day burn-in @ anode current of 50 μA, gain $= 2 \times 10^5$
15	Intrinsic rate effect	$< 1\%$ for current of 0.1 μA at gain $= 2 \times 10^5$
16	Single photoelectron resolution	> 1.5 peak/valley ratio on 1-pe peak

6 Electronics and Trigger

This section describes in detail the electronics which will be used to accumulate FPD data and construct an FPD trigger, whose existence we will communicate to the appropriate STAR trigger DSM to initiate the construction of a Level-0 STAR trigger and trigger token which we can associate with the FPD data. Except where indicated, all the electronics to be used for the FPD DAQ and trigger are currently located in-house at IUCF.

The requirements for the Tower PMT's and the MAPMT's as specified by the STAR EEMC group are listed in Tables 1 and 2, respectively. The Tower PMT's are EMI 9107B tubes with Cockcroft-Walton bases, as are envisioned to be used for the STAR endcap EMC.[10] The CW bases have low power consumption, and are well-suited to provide linear PMT operation for high peak currents that characterize the highest energy showers of interest. A group from Dubna is making the CW bases, and has previously designed and built similar systems before, capable of powering up to 10^4 PMT's, with voltages stable to 0.05% (read out to 10-bits) and dissipated power per channel of less than 0.12 W. Controls will be supplied through standard RS-232-C serial lines. The voltages will

Table 2: Table of requirements for the STAR endcap EMC MAPMT's.

Item	Description of parameter	Parameter value
1	# of anodes per phototube	16
2	MAPMT transverse dimensions	$\leq 30\,\mathrm{mm}$ square; photocathode active area $\geq 16\,\mathrm{mm} \times 16\,\mathrm{mm}$
3	MAPMT maximum length	40 mm without base
4	Dynode structure	11 or 12 stages, metal channel dynode
5	Photocathode	Bialkali, with QE $\geq 10\%$ @ 490 nm; Nonuniformity $< \pm 20\%$ over active area
6	Electrostatic shielding	Metal envelope held at cathode potential
7	Socket	Socket must be included
8	Maximum anode to cathode HV	$-1000\,\mathrm{V}$ DC
9	Anode pulse rise time	$\leq 5\,\mathrm{ns}$
10	Optimum average anode gain	$> 4 \times 10^5$ for all MAPMT's within $\Delta V = \pm 100\,\mathrm{V}$
11	Anode gain uniformity	Single pixel nonuniformity $< \pm 20\%$ within 1 mm of pixel center; max/min variation among anodes $\leq$ 2:1
12	Pulse nonlinearity	$\leq \pm 2\%$ for $0 \leq I_{peak} \leq 1\,\mathrm{mA}$ for each anode @ gain $= 4 \times 10^5$
13	Dark current	$< 0.5\,\mathrm{nA}$/channel @ gain $= 4 \times 10^5$
14	Crosstalk	Mean current in any nearest neighbor anode $< 2\%$, in any diagonal neighbor $< 1\%$ of illuminated anode
15	Magnetic field sensitivity	$< 50\%$ gain reduction in 30 G field transverse to MAPMT axis
16	PMT aging	$< 50\%$ gain reduction after 10-year exposure to total integrated charge of 2 C/anode
17	Long term instability (100 day period)	$< 5\%$ gain variation after initial burn-in @ gain $= 4 \times 10^5$

be controlled by a DAC made from the RC-filtered pulse-width modulation output of a PIC16C873 microcontroller. The controller will monitor HV, power consumption, and housing temperature with an internal 10-bit ADC, and will contain a high speed control logic FPGA whose configuration can be easily downloaded. The MAPMT's are Hamamatsu H6568 tubes, with 16 separate pixels available for each tube, with resistive bases from Hamamatsu made specially to fit with this multi-anode PMT geometry. The information on the tubes and bases is what is assumed at the time of the penning of this document.

The crates of electronics are housed in two existing racks, of dimensions $36'' \times 60'' \times 67''$, with a total weight of $\approx 500\,\mathrm{lbs}$. The power we will need for the entire FPD system is given by the specifications on the transformer box, which is housed in one of the racks, and is single-phase, 208 V with 5.25 kVA power draw (Control Power Co., catalog number 5MGX-5K-6-C). There is a 30 A breaker on this box.

We want to generate a bit to send to the STAR Trigger DSM on the response of the FPD to showers from high-energy photon pairs in an environment which includes a large flux of neutral and charged diffractive background, predominantly consisting of lower-energy hadrons, photons, and leptons. To eliminate much of this low-energy background, we plan simply to discriminate on the total amount of energy deposited in each tower, requiring the total energy to be above a programmable threshold set to be that which we expect from the deposition of a large amount of energy from photon showers in the detector. There are four detectors for which we need to sum the analog signals from the PMT's and then discriminate on the sum, that is, one set of twelve towers of the prototype EEMC and three sets of four Pb-glass detectors, denoted A, B, and C. The FPD trigger will then be defined as the inclusive OR of these four sums above threshold. From PYTHIA, the trigger rate from pp collisions producing large energy deposition (electromagnetic showers with $E > 30\,GeV$) in the pEEMC or Pb-glass detectors is expected to be $\approx 1\,\mathrm{Hz}$ at a luminosity of $5 \times 10^{30}\,\mathrm{cm}^{-2}\mathrm{s}^{-1}$. If the background environment at the planned position of the FPD is severe, the trigger rate can be maintained at 1 Hz simply by increasing the threshold.

So the route of the FPD signals to create the FPD trigger will look something like the schematic diagram in Figure 12.

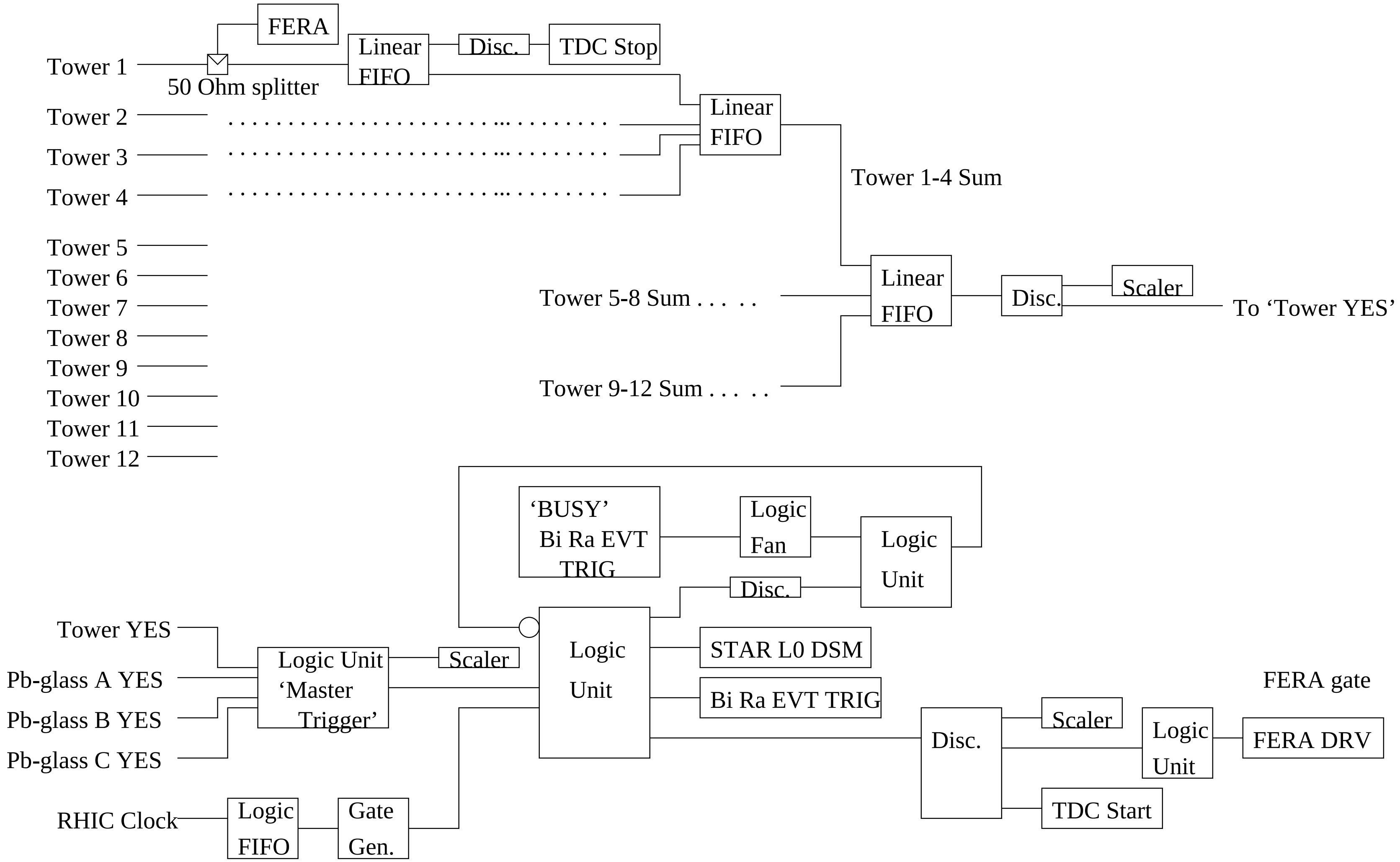

Figure 12: Schematic diagram of the FPD trigger.

The analog signals from each of the 12 Tower PMT's will be split by a $50\,\Omega$ passive splitter. One of these signals will go through a delay line into a LeCroy FERA 4300B module to encode the total charge and the other will feed into a linear fan-in/fan-out (FIFO) module. One of the outputs from this linear FIFO will go through a discriminator, and then will be delayed by $\approx 200\,\mathrm{ns}$ before eventually arriving as the TDC stop signal in a LeCroy 2228A TDC. The TDC start will have been generated by the RHIC clock in coincidence with an FPD trigger. The other output of the linear FIFO will go to cascading linear FIFO's together with the other tower PMT signals in order to create the sum of the tower PMT analog signals. Note that in order to do this, care must be taken with the timing of the analog signals to ensure their arrival at the cascading linear FIFO's will sum properly. One of these sums will be performed for the twelve tower PMT's, one for the Pb-glass detector array A, one for B, and one for C.

The pulse-height sums will go to a LeCroy 4413 sixteen channel discriminator, with its programmable threshold set to discriminate against energy deposition smaller than that produced by a large energy electromagnetic shower. If the total energy deposited in the prototype EEMC passes threshold, the signals from the discriminators will go into a LeCroy Model 2551 scaler and also into a logic coincidence unit (Phillips Scientific, PS Model 755), which is called the Master Trigger. We set the coincidence level of the Master Trigger at 1 for an inclusive-OR of the pEEMC, A, B, and C.

In the case of an 'FPD YES' from the FPD Master Trigger, we increment an (ungated) scaler, and send the 'FPD YES' to another logic coincidence unit (the "second PS755") to be ANDed with a 'not BUSY' signal from the FPD DAQ and with a 'RHIC clock' signal. The 'BUSY' signal is the result of either a fast 'BUSY' or a slow 'BUSY', ORed in a PS Model 757 mixed logic FIFO, the output of which goes back into the input of the second PS755. A fast 'BUSY' will have been generated by sending the output of the second PS755 through a LeCroy Model 821 quad discriminator and into the PS757. The slow 'BUSY' will come from a BiRa Model 2206 Event Trigger module, through a logic FIFO, and into the PS757. The 'RHIC clock' signal will come from the RHIC clock, sent through a separate PS757 mixed logic FIFO and into a LeCroy Model 222 gate generator, timed to be coincident with the photons incident on the FPD.

The ('FPD YES'$\cdot$'not BUSY'$\cdot$'RHIC clock') signal from the second PS755 will go to a BiRa Model 2206 Event Trigger, which tells the FPD VME processor to initiate the readout of all the appropriate FERA's and TDC's. In addition, a one bit signal will go to a Data Storage and Manipulation (DSM) board located in the trigger VME crate on the platform via a LEMO cable, where the STAR Level-0 trigger accept and trigger token will be constructed. We assume it takes approximately $15\,\mathrm{ns}$ for a signal to pass through each linear FIFO, discriminator, and logic coincident unit. With this assumption, once the PMT signals have arrived at the $50\,\Omega$ splitter, it will take $\approx 100\,\mathrm{ns}$ to generate the FPD trigger. Even with cable transit times, etc., the bit for the FPD trigger still will arrive in plenty of time to the STAR L0 trigger. More details on the interface with the STAR Trigger will be given in Section 8.

An ('FPD YES'·'not BUSY'·'RHIC clock') signal from the second PS755 will go to a (gated) scaler, and will also enable the generation of the appropriate gates to the FERA modules. This will be accomplished either by sending a NIM signal to a programmable gate and delay generator to set the same gate for all the FERA's, or by sending the NIM signal through a PS726 Level translator to obtain an ECL signal (on a twisted pair) with which we can send different gates to individual modules.

Once the event has been triggered in the BiRa2206 Event Trigger module, the slow 'BUSY' signal for the second PS755 will inhibit the generation of subsequent gates. We will receive the L0 accept, the action word, and the L2 accept from the FPD TCD module into a CAMAC I/O register (as used for the TOFp), incorporate the trigger token information into the header of the FPD event, and then ship it to the STAR DAQ. The FPD event data will be bussed to a VME crate, more specifically into a Creative Electronic Systems CBD 8210 module. In this VME crate will also be a Motorola MVME 712B module, whose output is an ethernet line which we will use to feed the FPD event into the STAR event stream. More details on the interface with STAR DAQ will be given in Section 8. At this point the 'BUSY' signal from the BiRa Event Trigger module will be cleared and we will be ready to accumulate the next event. The code to operate the VME modules will be downloaded from a Linux-PC.

We will have 160 pSMD channels of FERA information, 32 channels of FERA information from the preshower detector, 12 tower channels of FERA and TDC information, and 12 Pb-glass signals of FERA and TDC information, for a total of at most 240 channels for each event. The FERA data will be zero suppressed. On average we expect ~ 10 pSMD strips will contain data in a single event, resulting in an average number of channels equal to 90. At 11 bits per channel, the data for one FPD event correspond to ≈ 1000 bytes, so with additional room for headers and the trigger token, each FPD event will occupy approximately 1.2 kB/event.

7 High Voltage Details

The requirements for HV safety at RHIC have been extensively documented on the www at Reference [12].

We intend to provide power to the CW bases for the 12 tower PMT's with the "HVSys" system from Astakhov, *et al.* The HVSys system is the same as is used by the TOFp group to power their CW bases, and has been tested quite thoroughly by them, the details of which are well-documented in Reference [9]. This system has been observed to operate reliably and stably over periods of many months for the load at which they were tested. The load on the HVSys system for the FPD is less than the load that was used in these TOFp tests.

Power is provided through three main components of the HVSys system: a "System Module", by which one can control the system, a 10-conductor bus, through which HV control is communicated to the appropriate base, and HV "cells", which actually provide the voltage to the CW bases at the location of the bases, themselves. The idea behind the HVSys-CW base system is that at no point in the system do we have HV running along HV cables.

Control of the system is implemented through an HVSys System Module SM-255, located in the FPD electronics racks. The physical size of the System Module is designed according to the EUROMEKHANICS-6 U standard: 40 mm wide. The System Module connects only to the 10-conductor bus, to 110 V (60 Hz) AC power, and to a serial port for cell control and monitoring. The user control over the system is done either via a PC, using a dumb terminal program to send commands directly to the system module or a DOS-based GUI, or via RS-232-C protocol. Over the bus, the System Module provides the source voltage (200 V) which drives the CW bases, as well as the control and feedback signals. The bus is daisy-chained to each cell, up to a maximum length of 30 m, and the SM-255 module is able to control up to 64 HV cells per bus.

The HV cells are contained within the CW bases, and provide negative high voltage for the PMT's *within* the bases. To decrease the long-term effects of humidity, and for additional safety, the high voltage part of the cells is potted (the board of the two containing the CW multiplier chain of capacitors and diodes). The potting compond will be a standard commercial silicon encapsulant, such as Sylgard 182. The maximum (most negative) output voltage available to the CW bases is -1200 V, and the set voltage value is stable to 0.05%.

The voltage and current carried by the HVSys bus lines will be as follows. Of the 10 conductors, three conductors carry low voltage (one 200 V line, one 6 V line, and one -6 V line), three are power grounds, and four are signal lines for control and feedback ($0-5$ V and very low currents). The power drawn by a single cell under normal operating conditions is typically 0.1 W (0.35 W maximum).

The maximum power on the bus cable would occur if the bus had the maximum number of cells connected to it (64), in which case the typical(maximum) currents on the voltage lines would be 0.1(0.5) A on the 200 V line, 0.25(1.0) A on the ± 6 V lines. The FPD bus we propose will have only $12/64 \approx 20\%$ of the total number of cells that are possible on a single bus.

The ribbon cables chosen for this bus are Belden 2L26010 cables, which are rated to 300 V and 1.5 A, well above where we expect to run, typically. In addition, we will probably need to use an HVSys Bus Feedthrough connector on the back of the tower PMT box, which will be from, *e.g.*, AMP-LATCH Series 10 position feedthrough connectors with mating polarization and strain relief. To prevent overloading the ribbon cables, on the System Module there are two 1 A Wickmann fuses from Digi-Key on the ± 6 V lines. The 200 V line is protected by a current-limiting circuit in the System Module which ensures a maximum current of 0.25 A in case of a short circuit on this line. If this maximum current is sustained for more than 10 s, the System Module will switch off the 200 V line, which shuts down the system. On the cell side, the design of the CW bases prohibits HV currents of more than 2 mA on the last dynode, and 160 μA on the photocathode, which gives the aforementioned maximum 0.35 W power draw.

The tower PMT box will be grounded to the main ground bus directly as per National Electric Code standards. When grounding the tower PMT box to the main ground bus, care will have to be taken to prevent ground loops which could induce noise in the tower PMT's.

We intend to provide high voltage power to the 12 MAPMT's and the 12 Pb-glass PMT's with a LeCroy system HV4032A. This crate can hold up to eight so-called 3.3 kV pods of four channels each with negative polarity, for a total of 32 channels of HV. Individual channel control is available through a LeCroy Model 2132 CAMAC (IEEE-583) Interface. The voltage run-up and run-down rates are 1 kV/sec. The upper limit on the voltage for each channel is -3.3 kV and the current limit is fixed to be 3 ± 0.3 mA/channel. The ground for the HV will be from the electronics racks in which the HV crate is located, which will be attached directly to the main ground bus as per National Electric Code standards.

The HV power will be transported from the back of the HV modules to the MAPMT box via red jacketed RG-59B/U or RG-59/U shielded cables fitted with SHV male-connectors (Kings Electronics 1705-1). There is a panel on the back of the MAPMT box on which is mounted bulkhead SHV female-connectors for D hole mount type (Kings Electronics 1704-1), and can be seen in better detail in Figure 13. These bulkhead SHV connectors are mounted into a G-10 plane which is mounted with screws into the MAPMT box. The use of the G-10 allows the ground of the MAPMT bases to be separate from the ground of the MAPMT box. Within the MAPMPT box, the inner conductor is connected to a wire which has been specified by Hamamatsu especially for use with these MAPMT bases. This conductor connection is covered with black FIT heat shrinkable tubing from Alpha Wire Company, while the outer conductor (ground) is connected to these “Hamamatsu wires”, using unshielded Cu wire. The connection of the Hamamatsu HV wires to the MAPMT's can be seen coming from the right-hand side of Figure 14.

When in operation, the open end of the MAPMT box will be covered by a thick steel plate for magnetic shielding, as can be seen in Figure 15. With the thick steel plates in place, it is difficult to touch the HV connections within without really trying to stick one's fingers into the MAPMT box. However, in order to comply with appropriate safety regulations, we have the option to cover the openings in the MAPMT box/magnetic shielding assembly with wire mesh to prohibit fingers from being able to touch these HV connections. The mesh would cover the connections seen in Figure 13. As will be done for the tower PMT box, the MAPMT box will be grounded by a direct connection to the main ground bus as per National Electric Code standards, and care will have to be taken to prevent ground loops.

The 12 MAPMT's require approximately -1 kV, and the resistive bases have about 4 MΩ resistance, for a total power load of ≈ 0.25 W per channel. As mentioned before, the CW bases for the

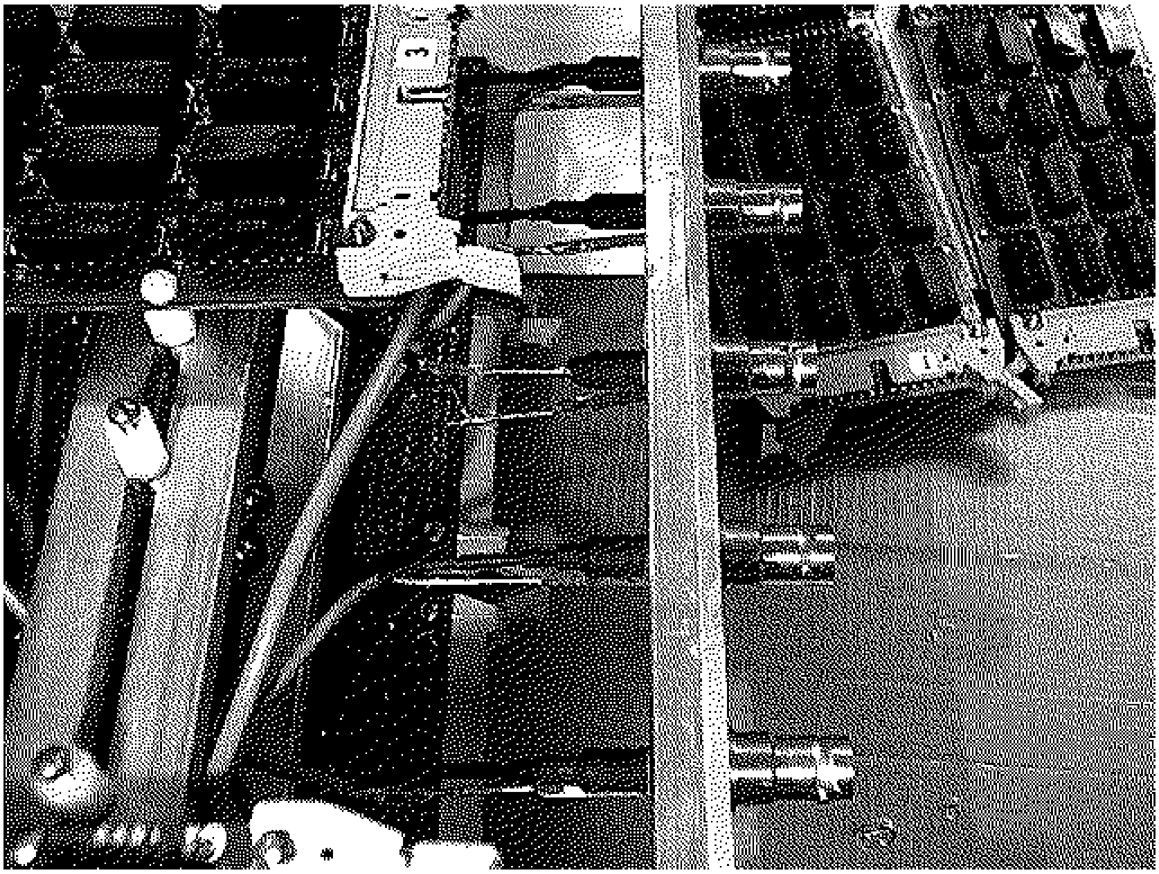

Figure 13: The SHV bulkhead connectors on the back of the MAPMT box with the connection to the Hamamatsu HV wires. Each bulkhead is mounted into the G-10 plane, which can be seen as the right-hand layer of material through which the SHV connectors pass. The inner conductor is connected to a Hamamatsu HV wire, which has been specified by Hamamatsu especially for use with these bases. The inner conductor and connection are covered with black shrink-wrap. The outer conductor (ground) and its connection are unshielded.

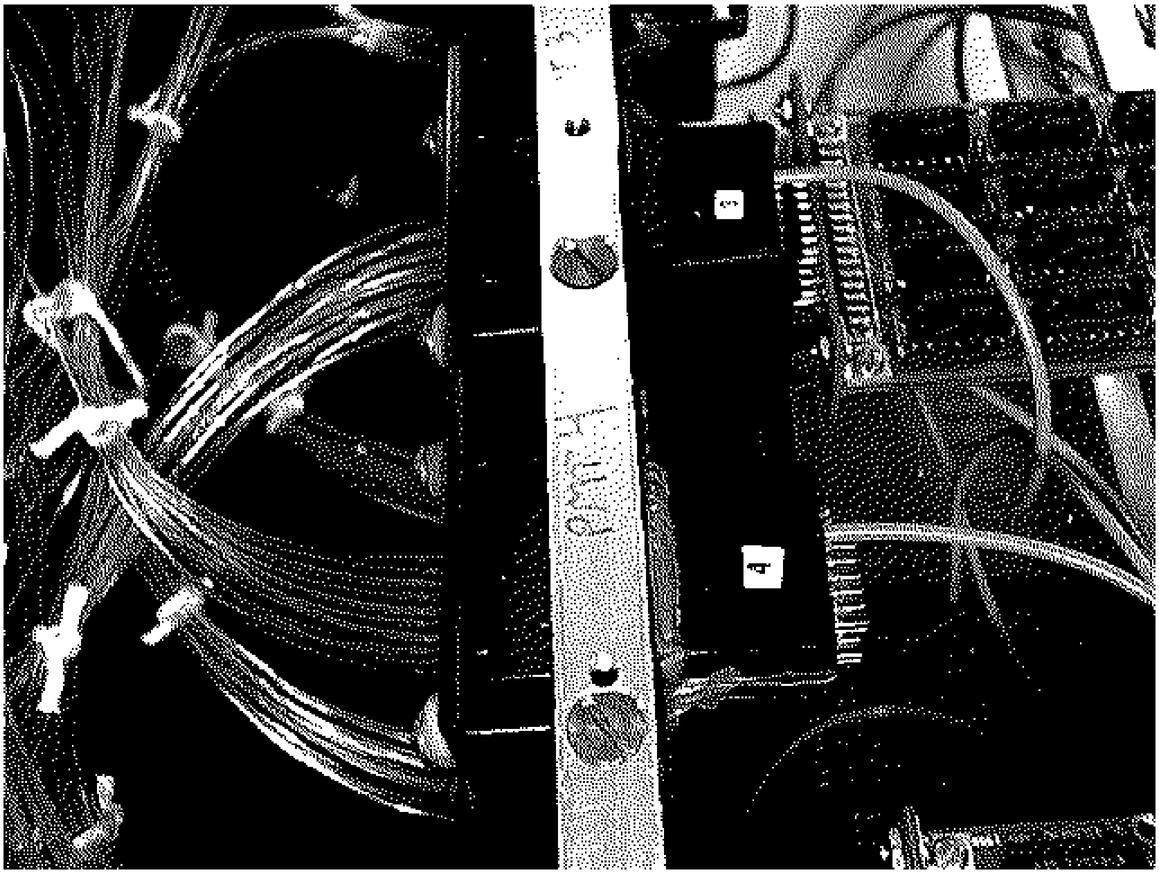

Figure 14: The Hamamatsu H6568 MAPMT's and bases. A delay board can be seen attached to the RHS of base "3." The clear fibers originating from the pSMD are coupled to pixels on the front-face of the MAPMT, and can be seen approaching the MAPMT from the LHS. The HV is supplied by the Hamamatsu HV wire, which is the thick wire entering the base from the RHS.

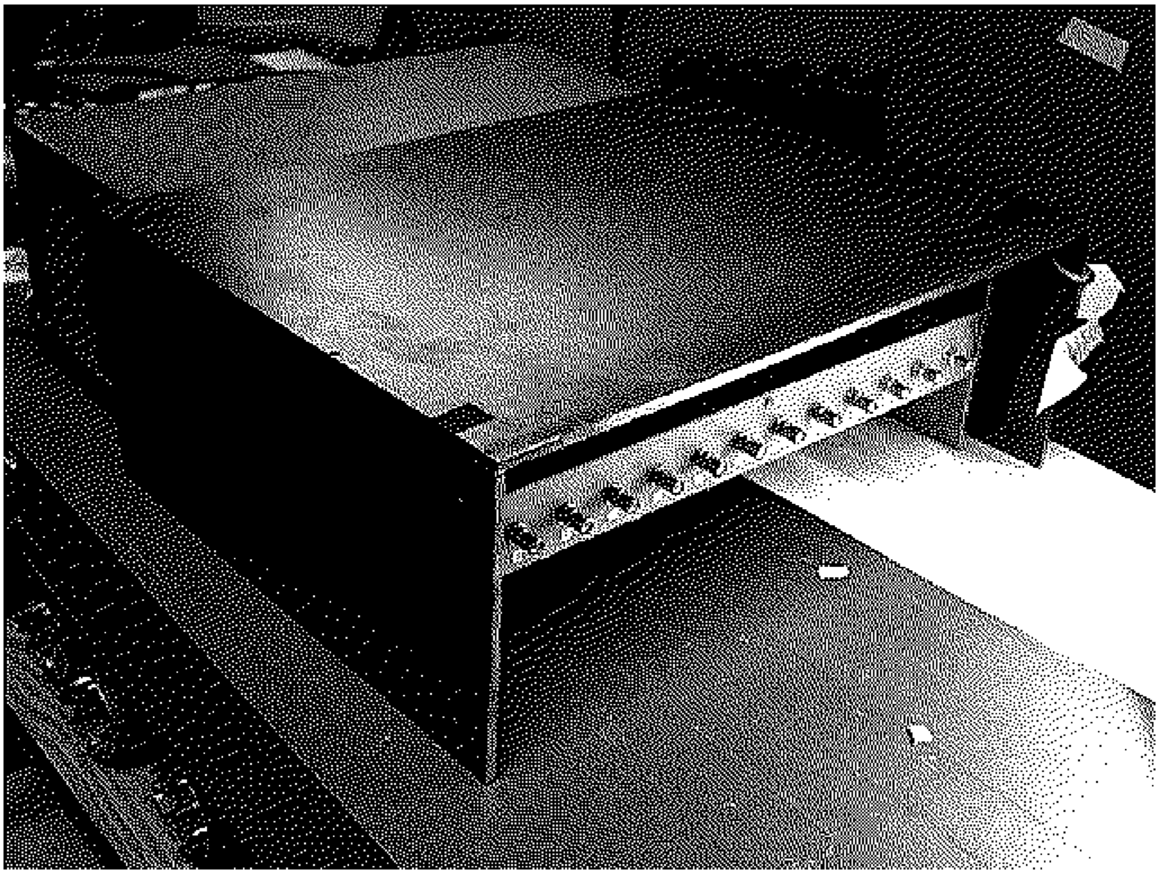

Figure 15: The MAPMT box, viewed from the back side, with the magnetic shielding in place.

12 tower PMT's typically have a power load of approximately 0.1 W. Altogether, this results in a total power draw of < 10 W for the entire FPD, so that we do not foresee the need for any additional cooling either at the electronics rack or at the detector.

8 Interface with STAR Level-0 Trigger and STAR DAQ

With the occurrence of a candidate π^0 event in the FPD which creates an FPD trigger as described in Section 6, we would like to write the FPD information to tape for further offline analysis. In addition, we would like to be able to have access to information available from the TPC which is coincident with our FPD event. Thus, it is important to be able to integrate into the standard STAR trigger and STAR event stream. The standard and sole event identifier for STAR is the STAR 12-bit trigger token. At the very least, it will be necessary to incorporate this token into the FPD data event header in order to be able to analyze these data offline in a sensible way.

The formation of a full STAR Level-0 (L0) trigger and token takes $\approx 1.5\,\mu$s, which is much longer than the time it will take to trigger the encoding of the FPD data. To communicate the existence of an FPD trigger as an L0 trigger, we will follow the scheme that is currently being used by the Zero-Degree Calorimeter (ZDC) group, and has been outlined by the Time-of-Flight patch (TOFp) group.[9] A 'YES' signal for an FPD L0 trigger comes from the second PS755 logic unit in the FPD DAQ, and will be communicated by way of a LEMO cable to one of the Data Storage and Manipulation (DSM) boards in the DSM tree (which also includes the CTB, for example) that is located in the trigger VME crate on the STAR platform. The field programmable gate array (FPGA) performs manipulations on the DSM tree and collects the detector bit information into a 12-18 bit word to send to a second module, called the Trigger Control Unit (TCU). The TCU looks at the bits from the DSM tree, determines the status of the BUSY, and decides if the physics is interesting, at which point it generates an L0-accept and the 12-bit trigger token. The L0-accept and the trigger token are passed along the back plane of the VME crate to a detector-specific Trigger Clock Driver (TCD), which will be microprogrammed to evaluate the information and see if the trigger is interesting for our detector. If so, the L0 trigger information is sent immediately to the FPD electronics via a twisted pair cable and a CAMAC I/O register.

The FPD Crate Controller must be programmed to periodically look at the appropriate CAMAC I/O register from the TCD bus. If an L0 is seen, the 12-bit trigger token for this event from the bus will be attached to the block of (already stored) FPD data corresponding to this same crossing. The FPD Crate Controller also must be programmed to periodically look for higher-level trigger aborts/accepts. If we receive a Level-2 abort, we will do a fast clear and then will be ready to accumulate another FPD event. If we receive a Level-2 accept, we are ready to be read into the main STAR data stream. A small header table will accompany the FPD data with the trigger token associated with this FPD event. This insures that the STAR DAQ can handle the FPD event, with its “proper papers.” The FPD DAQ system will be connected to the STAR DAQ system via an optical fiber link, as per the STAR DAQ standard.

In case something goes wrong with the above integration into the STAR DAQ, we can also write the data out to our own ntuple resident on the FPD DAQ computer. With the inclusion of the 12-bit trigger token from the STAR trigger, the event is uniquely identified and can be merged with STAR TPC information resulting from higher level triggers at a later time.

9 Safety

Safety issues which are involved with the installation and operation of the FPD are varied. It should be noted that the prototype EEMC has been already and will be again used at SLAC, another DOE facility with comparable regulations as are in place at BNL.

Regarding HV safety, see Section 7.

Regarding crush hazard from the pEEMC, the pEEMC will be supported on a sturdy table.

Regarding the handling of lead, there are members of the IUCF STAR-spin collaboration who have passed a Pb-safety course taken at IUCF, thus enabling them to handle lead, following proper procedures, at SLAC. It is envisioned that two people wearing gloves will handle each Pb radiator sheet, and take care to minimize direct exposure to the lead.

Regarding earthquake safety, there are four steel O-ring brackets bolted to the sides of the Al prototype box through which one can run a chain to attach to earthquake safety rigging. This was the configuration that was and will be again used at SLAC.

10 Installation Schedule, Manpower

We would like to install the FPD into its proposed position at BNL before the beginning of data taking for FY2001/2002, which is scheduled to begin 1 June 2001. At the moment, there are eight weeks dedicated for polarized p-p running during FY2001/2002 (three weeks of commissioning, five weeks of physics data) scheduled to take place from mid-August through mid-October. Currently, it is planned to test the prototype EEMC in a run at SLAC in January, 2001. After the SLAC run, we propose to install the prototype EEMC as the FPD at RHIC in March, 2001. From experience, the set up of the prototype EEMC and its associated electronics, from the time a truck arrived at SLAC with all of the equipment, took one week.

To install the FPD on this platform, it is envisioned that two people will carry the prototype box up to the west tunnel platform extension via a stairwell, without the Pb sheets inserted. Each Pb sheet can be carried individually up to the tunnel platform extension and slid into its rightful place in the FPD by two people wearing gloves.

All of the installation, including connecting all electrical components, timing the FPD DAQ, coordinating and performing the interfaces with STAR trigger and DAQ, etc., will be done by postdocs, research scientists, and professors from IUCF. We expect STAR to provide space on the west tunnel platform extension. We expect BNL to provide clean power and computer connections in the WAH for the FPD detector and DAQ. We expect the STAR trigger to provide a LEMO spigot for L0 input, accessibility to global trigger commands and tokens, and accessibility to subsequent accepts/aborts, as is done for the ZDC. We expect the STAR DAQ to provide us an ethernet connection to the STAR data stream, and some kind of 'READ OK' signal to indicate successful acceptance of the FPD data, as is done for the RICH.

References

[1] E.W. Hughes and R. Voss, Annu. Rev. Nucl. Part. Sci. **49**, 303 (1999).

[2] B. Adeva *et al.* (SMC Collaboration), Phys. Rev. D**58**, 112001 (1998) and Phys. Rev. D**58**, 112002 (1998).

[3] T. Gehrmann and W.J. Stirling, Phys. Rev. D**53**, 6100 (1996).

[4] "An Endcap Electromagnetic Calorimeter for STAR: Conceptual Design Report",

[5] D. L. Adams, *et al.*, Phys. Lett. B**261**(1991)201.

[6] D. L. Adams, *et al.*, Phys. Lett. B**264**(1991)462.

[7] J. Qiu and G. Sterman, Phys. Rev. D**59**(1998)014004.

[8] G. L. Kane, J. Pumplin, and W. Repko, Phys. Rev. Lett. **41**(1978)1689.

[9] "TOFp Technical Description", STAR TOFp Group, December 1999.

[10] "An Endcap Electromagnetic Calorimeter for STAR: Technical Design Update #1",

[11] R. Brown, private communication.

[12] See http://www.rhicadmin.bnl.gov/seappm/contents.htm.